Published in final edited form as:
Sci Signal. ; 4(201): rs13. doi:10.1126/scisignal.2002189.

SH3 Domain–Based Phototrapping in Living Cells Reveals Rho Family GAP Signaling Complexes

Hirokazu Okada[1], **Akiyoshi Uezu**[1], **Frank M. Mason**[1], **Erik J. Soderblom**[2], **M. Arthur Moseley III**[2], and **Scott H. Soderling**[1,*]

[1]Department of Cell Biology, Duke University Medical School, Durham, NC 27710, USA

[2]Institute for Genome Science & Policy Proteomics Core Facility, Duke University Medical School, Durham, NC 27710, USA

Abstract

Rho family GAPs [guanosine triphosphatase (GTPase) activating proteins] negatively regulate Rho family GTPase activity and therefore modulate signaling events that control cytoskeletal dynamics. The spatial distribution of these GAPs and their specificity toward individual GTPases are controlled by their interactions with various proteins within signaling complexes. These interactions are likely mediated through the Src homology 3 (SH3) domain, which is abundant in the Rho family GAP proteome and exhibits a micromolar binding affinity, enabling the Rho family GAPs to participate in transient interactions with multiple binding partners. To capture these elusive GAP signaling complexes in situ, we developed a domain-based proteomics approach, starting with in vivo phototrapping of SH3 domain– binding proteins and the mass spectrometry identification of associated proteins for nine representative Rho family GAPs. After the selection of candidate binding proteins by cluster analysis, we performed peptide array–based high-throughput in vitro binding assays to confirm the direct interactions and map the SH3 domain–binding sequences. We thereby identified 54 SH3-mediated binding interactions (including 51 previously unidentified ones) for nine Rho family GAPs. We constructed Rho family GAP interactomes that provided insight into the functions of these GAPs. We further characterized one of the predicted functions for the Rac-specific GAP WRP and identified a role for WRP in mediating clustering of the postsynaptic scaffolding protein gephyrin and the $GABA_A$ (γ-aminobutyric acid type A) receptor at inhibitory synapses.

Introduction

The Rho family small guanosine triphosphatases (GTPases), which include Rho, Rac, and Cdc42, function as molecular switches that cycle between guanosine triphosphate (GTP)–bound active forms and guanosine diphosphate (GDP)–bound inactive forms. In the active state, Rho family GTPases bind to effectors, such as kinases, formins, and the family of Wiskott-Aldrich syndrome proteins (WASPs), to form distinct actin cyto-skeletal structures that include linear bundled and branched networks of filaments. By governing the assembly and disassembly of these actin structures, Rho family GTPases regulate various cellular activities such as cell migration, cell differentiation, cytokinesis, intracellular membrane trafficking, angiogenesis, and neuronal morphogenesis such as axonal guidance and synapse

*To whom correspondence should be addressed. s.soderling@cellbio.duke.edu.

Author contributions: S.H.S. and H.O. conceived the project; H.O., F.M.M., E.J.S., and A.U. performed the experiments and analyzed the data; S.H.S. supervised the entire project; H.O. and S.H.S. wrote the manuscript; E.J.S., M.A.M., and F.M.M. commented on and edited the manuscript.

Competing interests: The authors declare that they have no competing financial interests.

formation (1, 2). GEFs (guanine nucleotide exchange factors) promote the activation of Rho family GTPases by promoting the exchange of GDP for GTP, whereas GAPs (GTPase-activating proteins) turn them "off" by stimulating the intrinsic GTP-hydrolyzing activity of the GTPases to accelerate their conversion to the inactive form. Characterization of individual GAPs indicates that their activities are regulated by various mechanisms including protein-protein interaction, lipid binding, subcellular translocation, phosphorylation, and proteolytic degradation (3). GAPs for Rho family GTPases (Rho family GAPs) are composed of multiple modular domains, most of which have been identified as protein-protein interaction domains, lipid-binding domains, or enzymatic domains (4). This suggests that GAP interactions with proteins or lipids may modify Rho family GAP activities in coordination with other signaling pathways. SH3 (Src homology 3) domains are the most prevalent protein-protein interaction domains found in Rho family GAPs. Despite the likely importance of Rho family GAP SH3 domain interactions on Rho GTPase signaling, their binding partners are mostly unknown.

SH3 domains have a micromolar-range binding affinity [dissociation constant (K_d) of 1 to 200 μM] (5, 6). SH3 domain interactions with ligand can be transient and depend on the cellular context—such as stimuli that affect ligand availability (6, 7). Because SH3 domains have a relatively broad ligand selectivity motif, each SH3 domain is likely to interact with several ligand proteins in vivo. These competitive interactions are thought to enable crosstalk between signaling pathways and result in a high degree of connectivity within a pathway. Such weak and transient interactions may therefore be crucial to the cellular roles of SH3 domain–containing GAP proteins. Conventional affinity purification methods may fail to detect transient or weak interactions because of cell extract preparation procedures or extensive washing. We performed in vivo phototrapping of SH3 domain–interacting proteins with a photoreactive amino acid cross-linker genetically incorporated into the proximity of the ligand-binding pocket of SH3 domains to identify SH3-ligand interactions in situ. We purified the cross-linked SH3-ligand complexes by a tandem affinity purification (TAP) strategy and identified the ligands by mass spectrometric analyses. We applied this methodology to the SH3 domains of 9 of the 14 human SH3 domain–containing Rho family GAPs. The interactions were verified by peptide array–based in vitro binding assays and coimmunoprecipitation experiments. Finally, we constructed protein interaction maps for each GAP to obtain mechanistic insights into their possible cellular functions. We found that WRP [WAVE (WASP family verprolin-homologous protein)– associated Rac GAP] binds to the principal inhibitory synapse scaffolding protein, gephyrin, and facilitates the postsynaptic clustering of gephyrin and ionotropic γ-aminobutyric acid type A ($GABA_A$) receptors. These results demonstrate the physiologic relevance of interactions identified by our approach and suggest that the WRP and gephyrin interaction may provide a mechanism to facilitate organization of receptors and signaling proteins at inhibitory synapses.

Results

Photo–cross-linking of ligands for Rho family GAP SH3 domains

To identify Rho family GAP–containing protein complexes organized by SH3 domains, we developed a multistep workflow (Fig. 1A) based on an initial screen that used photo-induced trapping of intracellular interactions. *p*-Benzoyl-L-phenylalanine (pBpa) is a phenylalanine derivative that is a highly efficient and highly specific photo-activatable cross-linker (8, 9) that can be translationally inserted into proteins of interest in mammalian cells (10–14). pBpa can be incorporated into proteins of interest in a site-specific manner through the concomitant expression of the pBpa-specific variant of *Escherichia coli* tyrosyl-$tRNA^{Tyr}$ (*Eco*-pBpaRS) and *Bacillus stearothermophilus* suppressor $tRNA^{Tyr}$ (Fig. 1B). We cloned Rho family GAP SH3 domains into a mammalian expression vector that coexpressed *Eco*-pBpaRS and the suppressor $tRNA^{tyr}$ and covalently trapped protein interactions in cells

transfected with this construct by flowing suspended cells through a chamber with a 350- to 365-nm light source (Fig. 1C). We attached a TAP tag to the SH3 domain to enable the purification of the resulting SH3 domain–ligand complexes with a high signal-to-noise ratio (Fig. 1D). We incorporated pBpa into nine SH3 domains (Fig. 2A). To effectively cross-link the SH3 domain to ligands, pBpa must be located near the ligand-binding pocket; however, pBpa should not replace an amino acid directly involved in the binding interaction. We selected two candidate amino acid positions on the basis of structural data for the SRGAP1 SH3 domain (Fig. 2B) (15). These sites were proximal to the ligand-binding pocket but showed little conservation in sequence alignments, suggesting that they are less likely to be critical for ligand interactions (Fig. 2A, yellow highlights). To investigate whether pBpa successfully cross-linked to potential SH3 ligands in vivo, we expressed the modified SRGAP2 SH3 domain in mammalian cells in the presence of pBpa. Exposure to ultraviolet (UV) light produced a number of high–molecular weight species, indicating that light induced pBpa-mediated cross-linking of ligands to the SH3 domain (Fig. 2C), whereas no cross-linking was apparent in the absence of light (Fig. 2D). To purify the cross-linked complexes, we transfected FreeStyle 293 cells with the modified SRGAP2 SH3 domain and added pBpa (1 mM). Three days after transfection, we exposed the cells to 350- to 365-nm light in a modified cross-linking chamber to induce phototrapping of potential SH3 ligands, lysed them, and isolated the SH3 domain and co-purifying proteins by TAP (Fig. 2E). We subjected the purified samples to tryptic digestion and identified the proteins linked to the SH3 domain by liquid chromatography and tandem mass spectrometry (LC-MS/MS).

Hierarchical clustering of MS-identified SH3-interacting proteins

Expression of the nine SH3 domains was rescued by coexpression of the suppressor transfer RNA (tRNA) and tRNA synthetase, although the abundance of the different proteins varied (fig. S1). SH3 expression, cross-linking, and purification were performed in duplicate with the nine Rho family GAP SH3 domains shown in Fig. 2A, and interacting proteins were identified by LC-MS/MS analysis. A total of 860 interacting proteins were identified with a stringency scoring threshold [1.6% peptide and 14.2% protein false discovery rates (FDRs)] aimed at minimizing the number of potential false negatives likely to occur at higher stringency. This lower-stringency candidate interactor list was used as the basis for additional interaction validations to generate higher-confidence interaction data (see below). The relative abundance of the candidate SH3 domain interactors in each sample was evaluated by a modified spectral counting method (16, 17). To decode the pattern of associated proteins for each of the nine bait SH3 domains, we hierarchically clustered the identified proteins with unbiased Pearson correlation based on the mean normalized spectral counts (Fig. 3A) (18). This clustering enabled a rapid categorization of the proteins into two groups: one group that was predominantly associated with a single SH3 domain and a second group that showed no propensities toward any specific bait. The second type likely represents nonspecific or false positives that may be common contaminants with all baits. We therefore focused on the first type of clusters, which we called protein interaction (PI) clusters, for further analyses (Fig. 3B). The association between each SH3 domain bait and the proteins in the corresponding PI cluster is of relatively high confidence because the other eight SH3 domain baits serve as negative controls. From the initial pool of 860 candidate proteins, we assigned 563 to PI clusters, substantially reducing the number of proteins to be further characterized. We assessed the abundance of proteins from the input cell lysate over a range of about three orders of magnitude (fig. S1C). Of the 563 proteins assigned to the nine PI clusters, only 10.8% were found in the input lysate (fig. S1D). Thus, most of the proteins identified in PI clusters appear to be low-abundance proteins that were enriched during the phototrap-based purification procedure.

SH3 domain ligand mapping by peptide array–based in vitro binding assay

The PI clusters contained not only proteins directly cross-linked to SH3 domains but also proteins that were stably associated with these cross-linked proteins. To identify those proteins that bound directly to the SH3 domains and to validate these interactions, we performed high-throughput in vitro binding assays (Fig. 4 and fig. S2, A to I). SH3 domains bind to proline-rich sequences containing a PXXP motif (where P is Pro and X is any amino acid) (6, 19). Because Rho family GTPases play a prominent role in regulating the cytoskeleton, we selected candidate proteins from the PI clusters that either had been implicated in cytoskeletal regulation or showed high spectral counts relative to other proteins in the cluster, and searched the sequences of those proteins for PXXP motifs. Peptides (18-mer) containing the PXXP motifs were synthesized on polyethylene glycol (PEG)–based cellulose membrane, incubated with purified glutathione *S*-transferase (GST)–tagged SH3 domains, and immunoblotted with an anti-GST anti-body, and binding strength, normalized to the strongest interaction for each SH3 domain, was quantified (fig. S2, A to I). Peptides that bound within the relative range of 5 to 100% of the strongest interaction for each SH3 domain were scored as positive. In the case of ARHGAP26, we syn-thesized 91 unique peptides from the 18 proteins listed in Fig. 3B in an array format [3 of the 18 proteins, C3orf10 (probable protein brick1), CYFIP1 (cytoplasmic FMR1-interacting protein 1), and NCKAP1 (Nck-associated protein 1), had no PXXP motifs]. The SH3 domain overlay showed binding to only nine unique peptides (Fig. 4, A and B), indicating that the SH3 domain interaction is highly specific. These peptides corresponded to sequences from five different proteins, MICAL1 (molecule interacting with CasL 1), PTK2 [protein tyrosine kinase 2, also known as focal adhesion kinase (FAK1)], ANKS1A (ankyrin repeat and sterile α motif domain–containing 1A), PKN3 (protein kinase N3), and RAB11FIP5 (Rab11 family interacting protein 5). The SH3 domain of ARHGAP26 is known to bind PTK2 and PKN3 (20, 21). Thus, the phototrapping of bound ligands with pBpa-modified SH3 domains retains the ligand preference of the wild-type domains and, moreover, can recapitulate known interactions. We further validated the interaction between ARHGAP26 and MICAL1, which, on the basis of spectral counts, was the most enriched protein in the ARHGAP26 PI cluster, in a co-immunoprecipitation assay with full-length constructs (Fig. 4C).

Analysis of peptides that bound directly to other GAP SH3 domains revealed multiple previously unidentified interactions (Fig. 4, D to F, and fig. S2, A to I). To verify that full-length proteins could recapitulate the SH3-peptide interactions, we tested several interactions by coimmunopre-cipitation using full-length constructs. We confirmed the peptide-based identification of interactions between Rho family GAPs and multiple types of proteins: (i) scaffold proteins gephyrin and SRGAP2 (Fig. 4G), palladin and SRGAP2 (fig. S2J); (ii) activators of actin polymerization WASF2 (Wiskott-Aldrich syndrome family protein 2, also referred to as WAVE2) and ARHGAP4 (Fig. 4H), DIAPH1 (diaphanous homolog 1) and ARHGAP4 (fig. S2K); and (iii) kinases activated by members of the Rho family, CDC42BPA (myotonic dystrophy kinase–related Cdc42-binding kinase) and SNX26 (Fig. 4I). These data confirmed that domain-based interactions can reproducibly identify complexes that exist between full-length proteins (22). Overall, 789 unique peptides from 163 proteins were screened with the peptide array. Positive binding, indicating direct ligands for the Rho family GAPs, was detected for 102 peptides (13%) from 54 proteins (33%). We identified 4 to 7 direct protein interactions for each SH3 domain except for RICS [Rho family GAP involved in β -catenin–*N*-cadherin and NMDA (*N*-methyl-D-aspartate) receptor signaling, also known as p250GAP], for which we identified 11 direct protein interactions. The result of the peptide array analyses, showing which candidate proteins interacted directly with each SH3 domain and providing the SH3 binding sequence for each protein, is summarized in Table 1.

Bioinformatic analyses to construct Rho family GAP interactomes

We next examined whether the proteins that interacted directly with each SH3 domain were likely to interact with other proteins in the corresponding PI clusters. Bioinformatic analysis was used to combine the direct SH3 domain interactions identified here (brown or orange edges) with previously known interactions (blue edges) among the proteins in the PI clusters (represented by circle nodes) (see Materials and Methods) (Fig. 5A and fig. S3, A to I). As illustrated for ARHGAP26 [Fig. 5A (left)], many of the proteins in the PI cluster interacted with one another, although most were only indirectly associated with the pertinent Rho family GAP. To identify possible cellular functions for each Rho family GAP, we characterized these interactomes further by focusing on the direct or primary binding interactions with each Rho family GAP and those proteins that were known to interact with these primary binders [Fig. 5, A (right) and B to I]. Cellular functions of some of proteins that interact directly with the SH3 domain (see Table 1) and their associated proteins have been identified, allowing us to infer the cellular functions in which each GAP may be involved. In most cases, multiple proteins that bound directly to a particular GAP had been implicated in the same functions, reinforcing the functional implications. Highlights from this network analysis are summarized below.

The SH3 domains of ARHGAP26 and ARHGAP10 are 68% identical and directly bind PTK2, a key kinase that promotes the turnover of focal adhesions, which are protein complexes that link extracellular matrix binding to signaling to the cytoskeleton (20, 23). We reproducibly identified ARHGAP26 (Fig. 5A, right) as a PTK2-binding protein in the present study. ARHGAP10 (Fig. 5B) instead bound to distinct focal adhesion elements: talin (TLN1), a critical structural component of the focal adhesion complex and ASAP2 [ArfGAP with SH3 domain, ankyrin repeat, and PH (pleckstrin homology) domain 2], which is a negative regulator of PXN (paxillin, an adaptor protein that organizes PTK2 and other proteins at focal adhesions) recruitment to focal contacts (24). These results suggest that ARHGAP26 and ARHGAP10 play different roles in focal adhesion assembly. ARHGAP26 also bound tightly to MICAL1, an actin filament disassembly factor activated downstream of semaphorin-plexin signaling (25), suggesting that ARHGAP26 may play a role in axonal pathfinding.

ARHGAP10L (Fig. 5C) bound to six proteins, including FHOD3 (a myocardial formin; formins stimulate actin polymerization downstream of Rho family GTPases), LRRFIP2 [leucine-rich repeat (in FLII) interacting protein], LMO7 (LIM domain only protein 7), and MYH14 (myosin14), all of which are highly expressed in skeletal muscle and heart. LRRFIP2 is associated with Flightless-1 (Fli-1), which enhances the activity of formin family proteins (26), implying a role of ARHGAP10L in FHOD3-mediated actin assembly that may be stimulated by Fli-1. LMO7 is required for normal heart development in zebrafish (27).

ARHGAP12 (Fig. 5D) localizes to cell-cell junctions in mouse epithelial tissues, including small intestine, kidney, salivary gland, and liver (28), but its function remains unknown. We found that ARHGAP12 bound to the tight junction component TJP2 [tight junction protein 2 or zona occlu-dens 2 (ZO2)]. Immunostaining of ARHGAP12 in human bronchial epithelial cells showed colocalization with TJP2 at tight junctions (fig. S3J). ARHGAP12 also bound to the kinase WNK1 (lysine-deficient kinase 1), which inhibits WNK4, a negative regulator of ion transport through tight junctions (29). These data suggest that ARHGAP12 may participate in tight junction formation and junctional ion transport.

ARHGAP4 (Fig. 5E), which is predominantly expressed in hematopoietic cells (30), bound to two distinct types of actin assembly activators, WASF2 and DIAPH1 (see Fig. 4H and fig. S2K for full-length coimmuno-precipitation). Moreover, ARHGAP4 SH3 domain

phototrapping identified most members of WASF2 complex [CYFIP1, cytoplasmic fragile X interacting protein 1), NCKAP1, ABI1 (Abl interacting protein 1), ACTR2 (actin-related protein 2), and ARPC2 (actin-related protein 2/3 complex subunit 2)], together with WASF2, as associated with ARHGAP4. DIAPH1 and WASF2 are also highly expressed in hematopoietic cells, where they are required for polarization and cell migration (31). These interactions indicate that ARHGAP4 negatively regulates actin polymerization in cells by forming complexes with WASF2 and DIAPH1, both of which are activated downstream of Rho family GTPases (31, 32). Consistent with this conclusion, the ARHGAP4-related GAPs, WRP and SRGAP2, bindtoWASF1 (also commonly known as WAVE1) and the formin FMNL1 (formin-like 1 protein), respectively, and oppose their actin polymerization and severing functions (33, 34).

SRGAP2 (Fig. 5F), a neuronal GAP, showed strong binding to an inhibitory synapse postsynaptic scaffolding protein, gephyrin, and an actin filament–bundling and remodeling protein, palladin (see Fig. 4G and fig. S2J for full-length coimmunoprecipitation). See below for our investigation of the functional link between gephyrin and SRGAP2 or the homologous WRP.

ARHGAP9 (Fig. 5G) is predominantly expressed in peripheral blood leukocytes, spleen, and thymus (35); its WW domain binds to mitogen-activated protein kinases (MAPKs) competitively within the MAPK kinase (MAPKK) binding site (36). Cell-based assays have shown that the ARHGAP9 and MAPK interaction suppresses epidermal growth factor receptor (EGFR)–induced actin reorganization, presumably by blocking MAPK activation (36). Our analysis identified the EGFR-associated protein EPS8 (EGFR pathway substrate 8) as bound to ARHGAP9. In addition to its own barbed-end actin capping activity, EPS8 stimulates mitogenic signaling to actin remodeling through SOS-1 (son of sevenless homolog 1), which functions as a GEF for Ras and Rac (37). EPS8 also interacts with BAIAP2 (brain-specific angiogenesis inhibitor 1–associated protein 2, also known as IRSp53) and facilitates Cdc42-mediated actin bundling, thereby promoting filopodial protrusion (38). ARHGAP9 may therefore connect MAPK and EPS8 signaling through ARHGAP9 SH3 domain–based interactions with EPS8.

SNX26 (sorting nexin 26, also called TCGAP or NOMA-GAP) (Fig. 5H), which, in both immature and adult mice, is predominantly expressed in the brain, inhibits the Rho GTPases TC10 and Cdc42 (39). SNX26 binds the receptor NTRK1 (neurotrophic tyrosine kinase receptor 1, also referred to as TrkA) and suppresses nerve growth factor (NGF)–induced neurite out-growth in a GAP-dependent manner (40, 41). NGF-induced NTRK1 activation causes ABL1 (c-Abelson kinase 1 or c-Abl)–mediated phosphorylation of the adaptor protein Crk at Tyr^{222}, resulting in the dissociation of paxillin and c-Abl from Crk (42), which is critical for NGF-induced neurite out-growth (43). Our analysis of the SNX26 SH3 domain identified c-Abl as a direct interaction, indicating a link between NGF signaling and Rho GTPase– mediated regulation of the cytoskeleton. We also identified two proteins involved in cell motility as SNX26-binding proteins: CDC42BPA, which facilitates myosindependent cell motility (44), and CAP1 (adenylyl cyclase– associated protein 1), which promotes the recycling of cofilin and actin for rapid actin turnover (45). CAP1-dependent facilitation of rapid actin turnover drives cell motility and may also bind to the Cdc42 GEF MCF2 (MCF.2 cell line transforming sequence) (45, 46). CAP1 is enriched in neuronal growth cones, and its depletion decreases growth cone Factin content and impairs neuronal outgrowth (47, 48). In *Drosophila*, CAP1 genetically interacts with c-Abl during axonal guidance (49). Thus, SNX26 may act downstream of NGF to coordinate TC10- and Cdc42-mediated responses with ABL1 and CAP1 signaling to promote neurite outgrowth.

RICS (Fig. 5I) is a brain-enriched GAP that inhibits dendritic spine formation and maturation (50, 51). RICS binds to subunit 2B (GRIN2B) of the NMDA-type glutamate receptor, and NMDA decreases RICS abundance. The NMDA-dependent decrease in RICS levels occurs principally through an increase in the microRNA miR132, which contributes to a decrease in RICS translation (52). We identified two proteases as RICS-binding proteins. One of these proteases, m-calpain (CAPN2), shows Ca^{2+}-dependent proteolytic activity upon NMDA-evoked Ca^{2+} influx, suggesting that RICS may also facilitate NMDA-dependent proteolysis of CAPN2 substrates within dendritic spines. Peptide array anal-ysis also revealed that RICS bound to CABLES1 (Cdk5 and ABL1 enzyme substrate), a scaffolding protein for two kinases, CDK5 (cyclin-dependent protein kinase 5) and ABL1. NMDA stimulates CAPN2 to cleave the CDK5-associated cofactor p35 (CDK5R1), thereby activating CDK5 (53). Thus, RICS may facilitate CDK5 activation by promoting a complex between CAPN2, CABLES, and CDK5. RICS also bound to another protease CTSB (cathepsin B), which may negatively regulate the abundance of another CABLES-associated protein, TP53 (tumor suppressor p53) (54).

Gephyrin clustering facilitated by WRP

To investigate the physiological relevance of the SH3 domain–mediated Rho family GAP interactions we identified, we characterized the interactions between SRGAP2 and the scaffolding protein gephyrin. Gephyrin contains two self-association domains, called the G and E domains (55). Together, these domains facilitate the organization of gephyrin clusters that anchor glycine and $GABA_A$ receptors at postsynaptic sites along the dendritic shaft (55). The formation of gephyrin clusters appears to depend on interactions between the gephyrin E domain and GABA or glycine receptors and probably involves local regulation of the actin cytoskeleton (56, 57). We found that SRGAP2 bound to the gephyrin E domain, suggesting that SRGAP2 may promote gephyrin clustering in vivo.

To test this possibility, we first performed a coimmunoprecipitation analysis. We used an antibody directed against gephyrin to precipitate complexes from mouse brain extract (MBE) and immunoblotted with an anti-body that recognizes both SRGAP2 and WRP, which share 90% identity in their SH3 domains (33, 34). SRGAP2 or WRP was readily detected in gephyrin immunoprecipitate from MBE, suggesting that SRGAP2, WRP, or both may interact with gephyrin in vivo (Fig. 6A). Coimmunoprecipitation of heterologously expressed WRP and gephyrin constructs from human embryonic kidney (HEK) 293 cells confirmed that WRP bound to gephyrin (fig. S4A); we also detected a weak association between gephyrin and WRP lacking the SH3 domain, indicating that indirect interactions between the two may also exist. In vitro peptide-binding assays revealed that the WRP and SRGAP2 SH3 domains bound to the same peptide in gephyrin (Fig. 6B). We had previously characterized WRP knockout mice as a potential model for 3p-syndrome mental retardation (a form of retardation resulting from microdeletions of chromosome 3p25-26) (58), and clustering gephyrin is induced by ARHGEF9, which is also associated with mental retardation (59, 60). Therefore, we focused on the potential role of WRP in gephyrin clustering. To assess WRP colocalization with gephyrin, we performed immunocytochemistry in HEK293 cells transfected with complementary DNAs (cDNAs) to express both. As previously shown in heterologous cells, gephyrin formed large clusters (Fig. 6C) (61). WRP co-localized with gephyrin at these clusters. Deletion of the WRP SH3 domain abolished colocalization, indicating that it depended on the SH3 domain (Fig. 6C). Because gephyrin clustering is relevant to its ability to cluster synaptic receptors, we examined the effect of WRP on the size of the gephyrin clusters. Coexpression of WRP with gephyrin increased the average size of gephyrin clusters by more than twofold compared to gephyrin alone (Fig. 6E). Distribution analysis showed that WRP decreased the fraction of clusters smaller than 4 μm^2 in area and increased the fraction of clusters larger than 6 μm^2

in area (Fig. 6F), suggesting that WRP induces or stabilizes gephyrin clustering. Immunocytochemical analysis of endogenous gephyrin in hippocampal neuronal cultures revealed punctate staining, which was mostly colocalized with VIAAT (vesicular inhibitory amino acid transporter), a presynaptic marker for inhibitory synapses (fig. S4B). Coexpression of green fluorescent protein (GFP)–tagged WRP increased the number of gephyrin clusters within the dendrite compared to that of GFP controls. Deletion of the SH3 domain abolished this effect, indicating that SH3 domain–dependent binding of WRP with gephyrin increased the dendritic clustering of gephyrin (Fig. 6, G and H).

Role of WRP in postsynaptic clustering of gephyrin and $GABA_A$ receptors in vivo

To confirm a role for WRP in mediating gephyrin clustering at synapses in vivo, we performed comparative histological analyses of gephyrin staining in the hippocampi of wild-type and WRP-knockout mice (58). Gephyrin is present in pyramidal neurons in the CA1 region of hippo-campal formation (62) (Fig. 7A). Therefore, we analyzed gephyrin staining within the stratum radiatum, where inhibitory synapses are formed on the dendrites of pyramidal cells. Consistent with the in vitro data, there was a decrease in the number of gephyrin clusters in WRP knockout mice compared to that of wild-type littermates (Fig. 7, B and C). Consistent with a role for gephyrin in promoting $GABA_A$ receptor clustering, the number of $GABA_A$ receptor puncta was decreased in WRP knockout mice (Fig. 7, B and D). Together, these data suggest that loss of WRP results in a decrease in gephyrin clustering and consequentially a reduction in $GABA_A$ receptor synaptic puncta. To determine whether the gephyrin clusters we analyzed were synaptic, we co-stained with VIAAT. Most of the gephyrin puncta colocalized with VIAAT immunopositive clusters, in-dicating that the gephyrin immunostaining was mainly synaptic (fig. S5). Because the density of VIAAT puncta was unaffected in WRP knockout mice, deletion of WRP does not appear to alter inhibitory innervation. This is consistent with studies showing that the deletion of other gephyrin-associated proteins such as ARHGEF9 or Neuroligin2 does not alter inhibitory presynaptic innervation (62, 63). To further analyze the effect of WRP on individual gephyrin and $GABA_A$ receptor clusters, we quantified the size of individual puncta. This analysis revealed that the average area of puncta was reduced for both gephyrin and $GABA_A$ receptors in WRP knockout mice (Fig. 7F). Together, these results, when combined with the overexpression data, suggest that WRP promotes clustering of postsynaptic $GABA_A$ receptors at inhibitory synapses.

Discussion

Our study has provided insight into how Rho family GAPs may organize the formation of complex signaling networks through SH3 domain interactions. The methodology described here is likely applicable to any proteomics-based approach that uses proteins where structural information is available to guide the placement of the pBpa. Indeed, a wide range of protein binding events may be identified by this approach, including protein-DNA interactions (64). We used an overexpression strategy, which undoubtedly increases the abundance of the bait proteins relative to that found in vivo. In the future, this technique could be refined by genetically modifying the locus for endogenous proteins such that the unnatural amino acid approach could be used in primary cells without over-expression of protein baits. However, our results demonstrate that the SH3 domain–based phototrapping approach can reveal new insights into physiologically relevant Rho family GAP signaling pathways.

Methodology

Affinity purification–MS/MS (AP-MS/MS) is commonly used to identify protein-protein interactions and is often a first approach toward the analysis of the cellular functions of

uncharacterized proteins (65). AP-MS/MS depends on stable interactions that can survive the multiple purification steps necessary for sample preparation. Many protein interactions are transient in nature or involve proteins of low abundance with micromolar binding affinities. These interactions may not be optimal for traditional AP-MS/MS approaches. Moreover, it is difficult to know whether interactions identified during standard purification approaches formed during lysis or actually occur within the intact cell. The methodology used here, in which protein interactions are covalently trapped in the intact cell, provides one approach for overcoming these limitations. Indeed, SH3 domains have a moderate (typically micromolar) binding affinity that enables multiple ligand interactions, some of which are likely to be transient. Only one protein identified by phototrapping and confirmed by peptide array analysis was also identified in the input lysate data (Talin-1 from the ARHGAP10 PI cluster) (Fig. 5B and fig. S1D). Thus, the interactions we identified through this approach appear to represent those of lower-abundance proteins that were enriched by phototrapping. Furthermore, the successful detection of interacting proteins relied on UV-dependent covalent cross-linking, because without cross-linking we only identified nonspecific interactions.

In addition to using pBpa to entrap and identify SH3-dependent interactions, we used several additional steps to distinguish specific from non-specific interactions. This included comparing the normalized abundance of proteins identified by MS from each SH3 domain bait to those of related SH3 domains. Proteins that were specifically enriched for an SH3 domain were considered to be candidate interacting proteins. This analysis reduced the number of possible interactions and enabled the generation of PI clusters for each SH3 domain. Further analysis using the peptide array–based binding assay revealed which of these proteins were likely to bind directly to each SH3 domain as well as the relative binding strengths and binding sites. These assays were done using the unmodified SH3 domain, indicating that binding interactions were not a result of altered specificity of the pBpa-containing domains. We also performed coimmunoprecipitation experiments with full-length proteins to validate a sample of the interactions we identified. All the interactions tested by coimmunoprecipitation were confirmed, suggesting that interactions identified by isolated SH3 domains were reliable. The success of this approach fits well with previous work showing that domain-based interaction studies can reliably recapitulate protein interactions that occur between full-length proteins (22).

By merging our interaction results for each SH3 domain with published protein association data, we obtained a more complete view of the possible protein networks organized around each Rho family GAP. These networks allowed us to predict possible functions for these GAPs based on the biological roles of their associated proteins. In most of the resulting networks, multiple proteins that had been previously implicated in the same functions were found for each Rho family GAP, increasing the likelihood that the predicted functional inference was correct. We also detected proteins in some networks that appeared to be outliers in that the function of these proteins did not seem to fit well with that of Rho family GAPs. These include histone regulatory protein (SMYD3 in Fig. 5G), splicing factors (SF1 and SF3B2 in Fig. 5E), or a negative regulator of telomerase activity (YLPM1 in Fig. 5F) (66). These interactions may represent false positives or interactions that are outside of our current understanding of the possible functions of these GAPs. One unexpected function predicted by our study that we confirmed, however, was the role of SRGAP2 (or the closely related WRP) in the postsynaptic architecture of inhibitory synapses.

Inhibitory synapse regulation by WRP

Relatively little is known about the postsynaptic structural proteins at inhibitory synapses. However, gephyrin, the most abundant scaffolding protein at inhibitory synapses, has long been thought to mediate the formation and maintenance of the postsynaptic organization of

receptors and signaling proteins (55). Gephyrin contains three major domains (G, C, and E domains). The G and E domains are believed to associate to form stable trimers or dimers, facilitating the clustering of gephyrin at postsynaptic sites that is also facilitated by other factors such as ARHGEF9 (55). However, the mechanisms that modulate the formation of these gephyrin clusters are not fully understood. We found that the Rac-specific GAPs SRGAP2 and WRP interact with gephyrin in vitro and in vivo. This interaction is likely to be physiologically relevant, because WRP increased the size and number of gephyrin clusters when over-expressed in HEK293 cells or in dissociated hippocampal neurons, whereas cluster size and number were decreased when WRP was knocked out in vivo. Our peptide array mapping study indicated that the SH3 domain of WRP binds to the gephyrin E domain, one of the domains responsible for gephyrin clustering. Both the actin filament and microtubule cytoskeleton have been implicated in gephyrin clustering (56, 57), and several cytoskeletal regulatory proteins interact with gephyrin, including the Cdc42 ARHGEF9 (55). ARHGEF9, by binding with neuroligin 2, promotes the translocation of gephyrin to the membrane (60–62, 67). Mice lacking ARHGEF9 exhibit region-specific decreases in the number of GABAergic in-hibitory synapses (63). However, neither ARHGEF9 GEF activity nor Cdc42 signaling plays a role in synaptic gephyrin clustering (68). Our results suggest that Rac signaling may contribute to gephyrin clustering, however, because WRP is selective for this GTPase (34). WRP has been implicated in a human 3p-syndrome mental retardation that in some, but not all, cases is associated with seizures (69). Mutations in WRP are also associated with schizophrenia, aspects of which may also be linked to altered GABAergic synaptic transmission (70–72). Thus, our discovery that loss of WRP in mice affects the postsynaptic structure of inhibitory synapses suggests a possible mechanism that could contribute to these neurological disorders associated with WRP mutations.

In summary, the data outline a new multistep approach for domain-based proteomics within cells that is applicable to many types of protein interactions. Using this approach, we identified possible roles for Rho family GAPs in numerous aspects of cell physiology, including the clustering of gephyrin at inhibitory synapses.

Materials And Methods

Plasmids

A mammalian expression vector that coexpresses the pBpa-specific variant of Eco-pBpaRS and B. stearothermophilus suppressor $tRNA^{Tyr}$ (a gift of S. Yokoyama, University of Tokyo) was modified for TAP (pcpBpaRSv4). A Strep-tag, followed by a calmodulin-binding peptide (CBP), a V5 epitope, a tobacco etch virus (TEV) protease cleavage site, and a tandem protein A tag, was inserted after a mammalian expression promoter. Unique Rsr II and Sbf I restriction sites were placed between CBP and V5 epitope for subcloning SH3 domain coding sequences.

The sequences of SH3 domains inserted and the amino acid residues mutated to amber codon are as follows: ARHGAP26 (amino acids 759 to 814, UniProt Q9UNA1, Ser^{773}), ARHGAP10 (amino acids 731 to 786, UniProt A1A4S6, Ser^{745}), ARHGAP10L (amino acids 820 to 874, UniProt A6NI28, His^{833}), ARHGAP9 (amino acids 25 to 87, UniProt Q9BRR9, Asp^{60}), SNX26 (amino acids 189 to 247, UniProt O14559, Asp^{203}), SRGAP2 (amino acids 725 to 786, UniProt O75044, Arg^{745}), ARHGAP4 (amino acids 749 to 804, UniProt P98171, Gln^{763}), RICS (amino acids 262 to 320, UniProt A7KAX9, Asp^{276}), and ARHGAP12 (amino acids 15 to 73, UniProt Q8IWW6, Asp^{49}). N-terminal GST fusion of the SH3 domains was made by subcloning an SH3 domain into pGEX-4T vector or cloning into pDEST15 vector with GATEWAY system (Invitrogen). GFP-tagged gephyrin and palladin, Flag-tagged ARHGAP4 and CDC42BPA, and Myc-tagged SNX26 were provided by M. Kneussel (University of Ham-burg, Germany), C. Otey (University of North

Carolina), T. Pawson (Mount Sinai Hospital, Canada), T. Leung (Institute of Molecular and Cell Biology, Singapore), and A. Saltiel (University of Michigan), respectively. WRP-V5, WRP(DSH3)-V5, GFP-WRP, and GFP-WRP(DSH3) constructs were previously described (34). SRGAP2-Flag and SRGAP2-V5 were also described (33). Gephyrin-V5 and MICAL-V5 were made by subcloning the open reading frames (ORFs) of mRNA sequences (BC030016 and NM022765, respectively) into pcDNA3.1-V5/His (Invitrogen). To make GFP-tagged ARHGAP26 and WASF2, we subcloned the ORF sequences into pEGFP-C2 vector with ARHGAP26 mRNA (BC068555) and the WASF2 plasmid previously described (73), respectively. All the amber mutants were generated following the QuikChange site-directed mutagenesis protocol (Stratagene).

Photo–cross-linking

For photo–cross-linking of the SRGAP2 SH3 domain variants (wild-type, R745amber, or D764amber) in Chinese hamster ovary (CHO) cells, the cells were transfected using Lipofectamine 2000 (Invitrogen) grown for 24 hours in growth medium containing 1 mM pBpa and exposed to UV light for 30 min with an 8-W handheld UV light before cell lysis. For photo–cross-linking of Rho family GAP SH3 domains in FreeStyle 293 cells, the following method was used. For transfection, a 1-liter culture of FreeStyle 293 cells was grown in FreeStyle 293 medium (Gibco) to the density of 1×10^6 cells/ml. Transfection was done following a modified polyethylenimine (PEI) protocol (74). One milligram of the vector DNA encoding TAP-tagged Rho family GAP SH3 domain plus Eco-pBpaRS and suppressor $tRNA^{Tyr}$ was mixed with 2 mg of PEI in 50 ml of FreeStyle 293 medium and added to the cell culture after 10 min of incubation. pBpa (270 mg) was dissolved in 1.1 ml of 1 M NaOH, filtered, and added to the cell culture dropwise after the addition of 7.5 ml of 1 M Hepes buffer to the culture. After a 3-day incubation at 37°C in the dark, the cells were transferred into a homemade cross-linking chamber, which was a commercially available "UV pond clarifier" (Garden Treasures, Home Depot) whose standard 254-nm UV bulb was replaced with a black light bulb (peak wavelength, 365 nm). After a 30-min photo-cross-linking in the chamber, cells were pelleted by centrifugation and either stored at −80°C or used for TAP purification.

Tandem affinity purification

The cross-linked cell pellet was resuspended in 20 ml of TAP lysis buffer [50 mM tris (pH 7.5), 150 mM NaCl, 1 mM EDTA, 7.5% glycerol, 25 mM NaF, 0.5% NP-40, 1 mM Na3VO4, 1 mM dithiothreitol (DTT), 1 mM 4-(2-aminoethyl)benzenesulfonyl fluoride hydrochloride (AEBSF), leupeptin/pepstatin (2 mg/ml)], homogenized with a Dounce homogenizer, and subjected to centrifugation at 17,200g for 30 min. The supernatant was further clarified by ultracentrifugation at 100,000g for 1 hour. The supernatant was mixed with prewashed immunoglobulin G (IgG)-Sepharose beads (200-μl bed volume) and incubated for 3 hours to overnight at 4°C. The beads were pelleted, resuspended with 0.5 ml of TAP lysis buffer, applied onto a chromatography column, and allowed to pack by gravity. After being washed with 50 ml of TAP lysis buffer and 5 ml of TEV cleavage buffer [10 mM tris (pH 7.5), 100 mM NaCl, 0.5 mM EDTA, 1% Triton X-100, 1 mM DTT, 1 mM AEBSF, leupeptin/pepstatin (2 μg/ml)], the beads were transferred into an Eppendorf tube, resuspended with 0.2 ml of TEV cleavage buffer, and incubated with 100 U of TEV protease for 3 hours at room temperature and overnight at 4°C. The whole solution was applied onto a new chromatography column, and the flow-through was collected. Residual eluate was further collected by applying 150 μl of TEV cleavage buffer four times to the column. Elution fractions were combined and mixed with prewashed calmodulin-Sepharose beads (400-ml bed volume) in 1 ml of 2× CBP-binding buffer [10 mM tris (pH 7.5), 100 mM NaCl, 2 mM MgAc, 4 mM CaCl2, 2 mM imidazole, 0.1% NP-40, 1 mM DTT, 1 mM AEBSF, leupeptin/pepstatin (2 μg/ml)], and incubated for 2 hours to overnight at 4°C. The

mixture was applied onto a new chromatography column. After being washed with 20 ml of calmodulin-rinsing buffer [50 mM ammonium bicarbonate (pH 8.0), 75 mM NaCl, 1 mM MgAc, 2 mM CaCl2, 1 mM imidazole, 1 mM AEBSF, leupeptin/pepstatin (2 mg/ml)] and 2 ml of 50 mM ammonium bicarbonate, the column was incubated with prewarmed calmodulinelution buffer [50 mM ammonium bicarbonate (pH 8.0), 25 mM EGTA] containing 0.1% RapiGest for 10 min and eluted. This was repeated three times with calmodulinelution buffer without RapiGest for 5 min. The eluates were combined and concentrated with an Amicon Ultra-4 [30,000 molecular weight cutoff (MWCO)] centrifugal filter device (Millipore) by centrifugation at 2500g for 5 min followed by the addition of 4 ml of 50 mM ammonium bicarbonate and centrifugation at 2500g for 10 min. The final sample contained the purified bait SH3 domain as well as the cross-linked species. One advantage of the relatively small SH3 domain, when compared to full-length bait proteins, is that the number of trypsin peptides in the sample from the bait domain was limited. This prevented the obscuring of the prey peptides by excess bait peptides during the subsequent MS identifications.

Sample preparation and nanoflow liquid chromatography electrospray ionization MS/MS analysis

After a total protein quantitation by a Bradford assay (Bio-Rad), samples were reduced with 5 mM DTT for 30 min at 70°C, and free sulfhydryls were alkylated with 10 mM iodoacetamide for 45 min at room temperature. Proteolytic digestion was accomplished by the addition of 500 ng of sequencing-grade trypsin (Promega) and incubation at 37°C for 18 hours. Samples were then acidified to pH 2.5 with trifluoroacetic acid (TFA) and incubated at 60°C for 1 hour to hydrolyze remaining RapiGest surfactant. Insoluble hydrolyzed surfactant was cleared by centrifugation at 15,000 rpm for 5 min.

Chromatographic separation of peptide mixtures was performed on a Waters nanoACQUITY UPLC equipped with a 1.7-μm BEH130 C18 reversed-phase column [75 μm inside diameter (ID) × 250 mm]. The mobile phase consisted of (A) 0.1% formic acid in water and (B) 0.1% formic acid in acetonitrile. After a 5-μl injection (1 μg of total peptide), peptides were trapped for 5 min on a 5-μm Symmetry *C18* column (180 μm ID× 20 mm) at 20 μl/min in 99.9% A. The analytical column was then switched inline and a linear elution gradient of 5% B to 40% B was performed over 90 min at 300 nl/min. The analytical column was connected to a fused silica PicoTip emitter (New Objective) with a 10-μm tip orifice and coupled to the mass spectrometer through an electrospray interface.

MS data were acquired on an LTQ-Orbitrap XL (TAP pull-downs and FreeStyle 293 lysate) (Thermo Scientific), QToF Premier (TAP pull-downs) (Waters), or QToF Ultima (TAP pull-downs) (Waters) mass spectrometer operating in positiveion electrospray ionization mode. For data acquired on the LTQ-Orbitrap XL, the instrument was set to acquire a precursor MS scan in the Orbitrap from mass/charge ratio *(m/z)* 400 to 2000 with $r = 60{,}000$ at m/z 400 and a target AGC setting of 1 × 10 ions. In a data-dependent mode of acquisition, MS/MS spectra of either the five (TAP pull-down) or two (293 lysate) most abundant precursor ions were acquired in the Orbitrap at $r = 7500$ at m/z 400 with a target AGC setting of 2×10^5 ions. Maximum fill times were set to 1000 ms for full MS scans and 500 ms for MS/MS scans with minimum MS/MS triggering thresholds of 5000 counts. For all experiments, fragmentation occurred in the LTQ linear ion trap with a collision-induced dissociation (CID) energy setting of 35% and a dynamic exclusion of 60 s was used for previously fragmented precursor ions. For data acquired on the QToF Premier or QToF Ultima, the instrument was set to acquire a precursor MS scan from m/z 50 to 1990 followed by three data-dependent MS/MS product ion scans from m/z 50 to 1990 with a charge state-dependent CID energy setting. To increase coverage of lower-abundance precursor ions, we used a 120-s dynamic exclusion list. A separate LC channel with Glu-1–fibrinopeptide (200

fmol/m l) in 50% acetonitrile/0.1% formic acid flowing at 500 nl/min was referenced every 30 s through a nano lock-spray interface.

Qualitative identifications from raw LC-MS/MS data

Raw LC-MS/MS data files were processed in Mascot distiller (Matrix Science) and then submitted to independent Mascot database searches (Matrix Science) against SwissProt and National Center for Biotechnology Information (NCBI) databases *(Homo sapiens* taxonomy) containing both forward and reverse entries of each protein. Search tolerances for LTQ-Orbitrap XL data were between 5 and 10 parts per million (ppm) for precursor ions and 0.02 dalton for product ions depending on the instrument performance as determined by a system suitability test of 50 fmol of yeast alcohol dehydrogenase digest run immediately before each sample. Search tolerances for QToF Premier and QToF Ultima data were 20 ppm for precursor ions and 0.04 dalton for product ions. All data were searched using trypsin specificity with up to two missed cleavages. Carbamidomethylation (+57.0214 daltons on C) was set as a fixed modification, whereas oxidation (+15.9949 daltons on M) was considered a variable modification. All searched spectra were imported into Scaffold (Proteome Software), and low-stringency protein confidence thresholds were set with a Bayesian statistical algorithm based on the PeptideProphet and ProteinProphet algorithms, which yielded a peptide and protein FDR of 1.6% and 14.2%, respectively (75, 76).

Hierarchical clustering

Relative protein abundance in the sample prepared by TAP was quantified with spectral counting *(*16*).* We used “quantitative values” calculated within Scaffold to provide a first-pass normalization of spectral counts for each protein based on the average total spectra counts across multiple samples (17). To further normalize the relative protein abundance, we expressed the (modified) spectral counts as a percentage of the total spectra observed in the sample. Mean normalized spectral counts were obtained from multiple independent experiments ($n \geq 2$ for each Rho family GAP). Hierarchical clustering was performed on the basis of the uncentered Pearson correlation of the mean normalized spectral counts by means of the Cluster 3.0 program (http://bonsai.ims.utokyo.ac.jp/~mdehoon/software/cluster/) (77). The dendrograms were viewed with the Java TreeView program (http://jtreeview.sourceforge.net/) (78).

Peptide array synthesis and SH3 domain overlay

Peptides (18-mer) were synthesized as previously described (34) with Auto Spot Robot ASP 222 (Intavis AG). GST-tagged SH3 domain over-lays were performed with 100 μM protein as previously described (73). Immunopositive peptide spots were densitometrically quantified with MetaMorph (version 7.7) (http://www.moleculardevices.com/).

Construction of interactomes

Rho family GAP protein-protein interaction networks were constructed by combining the SH3 domain–ligand interactions revealed through this study and previously known (physical) interactions. The known (physical) interactions were searched among (i) proteins identified in the PI clusters predominantly associated with individual Rho family GAP SH3 domains, (ii) subspecific proteins that showed association to two Rho family GAP SH3 domains only (including the focused Rho family GAP SH3 domain), and (iii) GTPases (RhoA, Cdc42, Rac1), using GeneMANIA (version 2.0) (http://genemania.org/), Ingenuity (http://www.ingenuity.com/), and STRING (version 8.3) (http://string-db.org/) (79). The open-source platform Cytoscape (version 2.8.0) was used to visualize the protein-protein networks (http://www.cytoscape.org/).

Immunostaining of cell lines and cultured neurons

HEK293 cells were maintained in Dulbecco's modified Eagle's medium (DMEM) supplemented with 10% fetal bovine serum (FBS) and penicillin/streptomycin. The cells were plated onto poly-D-lysine–coated glass cover-slips and transfected with GFP-gephyrin and vector or WRP-V5 by means of Lipofectamine 2000 (Invitrogen), following the manufacturer's instruction. Two days after transfection, cells were washed with phosphate-buffered saline (PBS) and fixed for 10 min with 4% paraformaldehyde in PBS. Cells were then permeabilized for 3 min with 0.1% Triton X-100 in PBS. After being washed with PBS, the cells were incubated for 1 hour with blocking solution (10% normal goat serum in PBS) and incubated overnight at 4°C with monoclonal anti-V5 (Invitrogen, 1:200) in a blocking buffer containing 0.1% Triton X-100. After extensive washing, cells were incubated for 1 hour with Alexa-labeled secondary antibodies (Molecular Probes). Fluorescence signals were visualized with Zeiss 710 confocal laser scanning system (Zeiss). Confocal images (10× magnification) were randomly taken, and the cells observed in the images were analyzed with MetaMorph to quantify the area and fluorescence intensity of gephyrin clusters. Total 683 (Vector) or 326 (WRP-V5) of gephyrin clusters were measured from three independent experiments. To analyze gephyrin clustering in the neurons, we prepared hippocampal neuronal cultures from postnatal day 1 pups and transfected them with Lipofectamine 2000 (Invitrogen) as described previously (58). Neurons transfected at DIV9 (day 9 in vitro) with GFP, GFP-WRP, or WRP(DSH3) were fixed at DIV12 and processed for immunostaining as described above. The primary antibodies used are anti-gephyrin monoclonal antibody (mAb) (mAb7a, SYnaptic SYstems, 1:300) and polyclonal anti-GFP antibody (Invitrogen, 1:400) or polyclonal rabbit anti-VIAAT (vesicular GABA transporter) (SYnaptic SYstems, 1:500). Neurons that were positive for GFP were randomly selected [GFP, $n = 42$ cells from seven mice; GFP-WRP, $n = 27$ cells from four mice; GFP-WRP (DSH3), $n = 14$ cells from three mice], and the confocal images of neuronal dendrites (63× magnification) were taken on a Zeiss 710 confocal microscope. The length of dendritic segments was measured with ImageJ software (National Institutes of Health), and the number of gephyrin puncta in the dendritic segments overlapping with GFP signal was counted manually.

Immunoprecipitation experiments

Coimmunoprecipitation experiments were performed as previously described in detail (33, 34). Briefly, lysates were precleared before incubation with antibody and either agarose-conjugated protein A or G overnight at 4°C with rocking. Antibodies and bound proteins from extracts were pre-cipitated by centrifugation and extensively washed. Bound proteins were eluted in SDS sample buffer.

Statistical analysis

Statistical analysis, Student's *t* test (two-tailed), was done with 2007 Office Excel version 12.

Animals

Description of the WRP knockout animals has previously been published (58). These mice contain a LoxP flanked exon 3, allowing for conditional deletion upon Cre recombinase expression. Mice used in this study were from previous crosses into a cytomegalovirus (CMV)-based Cre transgenic line to create germline deletion of the WRP exon 3. All mice were housed in Duke University's Division of Laboratory Animal Resources facilities, and all procedures were approved by the Duke University Institutional Animal Care and Use Committee and were in accordance with National Institutes of Health guidelines.

Immunostaining of brain sections

Preparation of brain sections was as previously described (80) with some modifications. Briefly $WRP^{+/+}$ and $WRP^{-/-}$ P40 mice ($n = 3$ for each geno-type) were anesthetized and decapitated. The brains were rapidly excised and frozen in dry ice. Cryostat sections (30 μm thick) were mounted onto gelatin-coated slides and briefly fixed with precold 2% paraformaldehyde/PBS solution for 10 min. The sections were subjected to antigen retrieval in citrate buffer [10 mM citric acid and 0.05% Tween 20 (pH 6.0)] before being incubated overnight with antibodies against mAb7a (SYnaptic SYstems, 1:200) and polyclonal rabbit anti-$GABA_A$ receptor γ2 subunit (SYnaptic SYstems, 1:300). For each mouse, four brain slices were processed for immunostaining. Quantification of gephyrin and GABA receptor puncta densities was performed with MetaMorph on two images per slice of the CA1 region of the hippocampus taken at a 63× magnification. The area and fluorescence intensity of puncta were quantified with “puncta analyzer” plug-in (written by B. Wark) for ImageJ (81). Adjacent sections to stain with anti-bodies against mAb7a and VIAAT (1:500) were treated in the same way.

Supplementary Material

Refer to Web version on PubMed Central for supplementary material.

Acknowledgments

We thank M. Sassoè-Pognetto (University of Turin) for the advice on immunohistochemistry; S. Yokoyama (University of Tokyo), M. Kneussel (University of Hamburg), C. Otey (University of North Carolina), T. Pawson (Mount Sinai Hospital), T. Leung (Institute of Molecular and Cell Biology), and A. Saltiel (University of Michigan) for the gifts of plasmids. We also thank W. Thompson and M. Turner (Duke University) for help with the lysate expression analysis and for MS sample preparation.

Funding: This work was supported by NIH grants R21-CA-140030–01 and R01-NS059957 (S.H.S.).

References and Notes

1. Van Aelst L, D'Souza-Schorey C. Rho GTPases and signaling networks. Genes Dev. 1997; 11:2295–2322. [PubMed: 9308960]
2. Symons M, Settleman J. Rho family GTPases: More than simple switches. Trends Cell Biol. 2000; 10:415–419. [PubMed: 10998597]
3. Tcherkezian J, Lamarche-Vane N. Current knowledge of the large RhoGAP family of proteins. Biol Cell. 2007; 99:67–86. [PubMed: 17222083]
4. Bernards A, Settleman J. GAP control: Regulating the regulators of small GTPases. Trends Cell Biol. 2004; 14:377–385. [PubMed: 15246431]
5. Mayer BJ. SH3 domains: Complexity in moderation. J Cell Sci. 2001; 114:1253–1263. [PubMed: 11256992]
6. Li SS. Specificity and versatility of SH3 and other proline-recognition domains: Structural basis and implications for cellular signal transduction. Biochem J. 2005; 390:641–653. [PubMed: 16134966]
7. Robens JM, Yeow-Fong L, Ng E, Hall C, Manser E. Regulation of IRSp53-dependent filopodial dynamics by antagonism between 14-3-3 binding and SH3-mediated localization. Mol Cell Biol. 2010; 30:829–844. [PubMed: 19933840]
8. Kauer JC, Erickson-Viitanen S, Wolfe HR Jr, DeGrado WF. *p*-Benzoyl-L-phenylalanine, a new photoreactive amino acid. Photolabeling of calmodulin with a synthetic calmodulin-binding peptide. J Biol Chem. 1986; 261:10695–10700. [PubMed: 3733726]
9. O'Neil KT, Erickson-Viitanen S, DeGrado WF. Photolabeling of calmodulin with basic, amphiphilic a-helical peptides containing *p*-benzoylphenylalanine. J Biol Chem. 1989; 264:14571–14578. [PubMed: 2760074]

10. Hino N, Okazaki Y, Kobayashi T, Hayashi A, Sakamoto K, Yokoyama S. Protein photo-cross-linking in mammalian cells by site-specific incorporation of a photoreactive amino acid. Nat Methods. 2005; 2:201–206. [PubMed: 15782189]
11. Farrell IS, Toroney R, Hazen JL, Mehl RA, Chin JW. Photo-cross-linking interacting proteins with a genetically encoded benzophenone. Nat Methods. 2005; 2:377–384. [PubMed: 16170867]
12. Wang W, Takimoto JK, Louie GV, Baiga TJ, Noel JP, Lee KF, Slesinger PA, Wang L. Genetically encoding unnatural amino acids for cellular and neuronal studies. Nat Neurosci. 2007; 10:1063–1072. [PubMed: 17603477]
13. Liu W, Brock A, Chen S, Schultz PG. Genetic incorporation of unnatural amino acids into proteins in mammalian cells. Nat Methods. 2007; 4:239–244. [PubMed: 17322890]
14. Sakamoto K, Hayashi A, Sakamoto A, Kiga D, Nakayama H, Soma A, Kobayashi T, Kitabatake M, Takio K, Saito K, Shirouzu M, Hirao I, Yokoyama S. Site-specific incorporation of an unnatural amino acid into proteins in mammalian cells. Nucleic Acids Res. 2002; 30:4692–4699. [PubMed: 12409460]
15. Li X, Chen Y, Liu Y, Gao J, Gao F, Bartlam M, Wu JY, Rao Z. Structural basis of Robo proline-rich motif recognition by the srGAP1 Src homology 3 domain in the Slit-Robo signaling pathway. J Biol Chem. 2006; 281:28430–28437. [PubMed: 16857672]
16. Liu H, Sadygov RG, Yates JR III. A model for random sampling and estimation of relative protein abundance in shotgun proteomics. Anal Chem. 2004; 76:4193–4201. [PubMed: 15253663]
17. Searle BC. Scaffold: A bioinformatic tool for validating MS/MS-based proteomic studies. Proteomics. 2010; 10:1265–1269. [PubMed: 20077414]
18. Eisen MB, Spellman PT, Brown PO, Botstein D. Cluster analysis and display of genome-wide expression patterns. Proc Natl Acad Sci USA. 1998; 95:14863–14868. [PubMed: 9843981]
19. Tonikian R, Xin X, Toret CP, Gfeller D, Landgraf C, Panni S, Paoluzi S, Castagnoli L, Currell B, Seshagiri S, Yu H, Winsor B, Vidal M, Gerstein MB, Bader GD, Volkmer R, Cesareni G, Drubin DG, Kim PM, Sidhu SS, Boone C. Bayesian modeling of the yeast SH3 domain interactome predicts spatiotemporal dynamics of endocytosis proteins. PLoS Biol. 2009; 7:e1000218. [PubMed: 19841731]
20. Hildebrand JD, Taylor JM, Parsons JT. An SH3 domain-containing GTPase-activating protein for Rho and Cdc42 associates with focal adhesion kinase. Mol Cell Biol. 1996; 16:3169–3178. [PubMed: 8649427]
21. Shibata H, Oishi K, Yamagiwa A, Matsumoto M, Mukai H, Ono Y. PKNb interacts with the SH3 domains of Graf and a novel Graf related protein, Graf2, which are GTPase activating proteins for Rho family. J Biochem. 2001; 130:23–31. [PubMed: 11432776]
22. Rual JF, Venkatesan K, Hao T, Hirozane-Kishikawa T, Dricot A, Li N, Berriz GF, Gibbons FD, Dreze M, Ayivi-Guedehoussou N, Klitgord N, Simon C, Boxem M, Milstein S, Rosenberg J, Goldberg DS, Zhang LV, Wong SL, Franklin G, Li S, Albala JS, Lim J, Fraughton C, Llamosas E, Cevik S, Bex C, Lamesch P, Sikorski RS, Vandenhaute J, Zoghbi HY, Smolyar A, Bosak S, Sequerra R, Doucette-Stamm L, Cusick ME, Hill DE, Roth FP, Vidal M. Towards a proteome-scale map of the human protein-protein interaction network. Nature. 2005; 437:1173–1178. [PubMed: 16189514]
23. Ren XR, Du QS, Huang YZ, Ao SZ, Mei L, Xiong WC. Regulation of CDC42 GTPase by proline-rich tyrosine kinase 2 interacting with PSGAP, a novel pleckstrin homology and Src homology 3 domain containing rhoGAP protein. J Cell Biol. 2001; 152:971–984. [PubMed: 11238453]
24. Kondo A, Hashimoto S, Yano H, Nagayama K, Mazaki Y, Sabe H. A new paxillin-binding protein, PAG3/Papa/KIAA0400, bearing an ADP-ribosylation factor GTPase-activating protein activity, is involved in paxillin recruitment to focal adhesions and cell migration. Mol Biol Cell. 2000; 11:1315–1327. [PubMed: 10749932]
25. Hung RJ, Yazdani U, Yoon J, Wu H, Yang T, Gupta N, Huang Z, van Berkel WJ, Terman JR. Mical links semaphorins to F-actin disassembly. Nature. 2010; 463:823–827. [PubMed: 20148037]
26. Higashi T, Ikeda T, Murakami T, Shirakawa R, Kawato M, Okawa K, Furuse M, Kimura T, Kita T, Horiuchi H. Flightless-I (Fli-I) regulates the actin assembly activity of diaphanous-related

formins (DRFs) Daam1 and mDia1 in cooperation with active Rho GTPase. J Biol Chem. 2010; 285:16231–16238. [PubMed: 20223827]

27. Ott EB, van den Akker NM, Sakalis PA, Gittenberger-de Groot AC, Te Velthuis AJ, Bagowski CP. The lim domain only protein 7 is important in zebrafish heart development. Dev Dyn. 2008; 237:3940–3952. [PubMed: 19035355]
28. Matsuda M, Kobayashi Y, Masuda S, Adachi M, Watanabe T, Yamashita JK, Nishi E, Tsukita S, Furuse M. Identification of adherens junction-associated GTPase activating proteins by the fluorescence localization-based expression cloning. Exp Cell Res. 2008; 314:939–949. [PubMed: 18241859]
29. Gamba G. Role of WNK kinases in regulating tubular salt and potassium transport and in the development of hypertension. Am J Physiol Renal Physiol. 2005; 288:F245–F252. [PubMed: 15637347]
30. Tribioli C, Droetto S, Bione S, Cesareni G, Torrisi MR, Lotti LV, Lanfrancone L, Toniolo D, Pelicci P. An X chromosome-linked gene encoding a protein with characteristics of a rhoGAP predominantly expressed in hematopoietic cells. Proc Natl Acad Sci USA. 1996; 93:695–699. [PubMed: 8570618]
31. Campellone KG, Welch MD. A nucleator arms race: Cellular control of actin assembly. Nat Rev Mol Cell Biol. 2010; 11:237–251. [PubMed: 20237478]
32. Takenawa T, Suetsugu S. The WASP–WAVE protein network: Connecting the membrane to the cytoskeleton. Nat Rev Mol Cell Biol. 2007; 8:37–48. [PubMed: 17183359]
33. Mason FM, Heimsath EG, Higgs HN, Soderling SH. Bi-modal regulation of a formin by srGAP2. J Biol Chem. 2011; 286:6577–6586. [PubMed: 21148482]
34. Soderling SH, Binns KL, Wayman GA, Davee SM, Ong SH, Pawson T, Scott JD. The WRP component of the WAVE-1 complex attenuates Rac-mediated signalling. Nat Cell Biol. 2002; 4:970–975. [PubMed: 12447388]
35. Furukawa Y, Kawasoe T, Daigo Y, Nishiwaki T, Ishiguro H, Takahashi M, Kitayama J, Nakamura Y. Isolation of a novel human gene, ARHGAP9, encoding a Rho-GTPase activating protein. Biochem Biophys Res Commun. 2001; 284:643–649. [PubMed: 11396949]
36. Ang BK, Lim CY, Koh SS, Sivakumar N, Taib S, Lim KB, Ahmed S, Rajagopal G, Ong SH. ArhGAP9, a novel MAP kinase docking protein, inhibits Erk and p38 activation through WW domain binding. J Mol Signal. 2007; 2:1. [PubMed: 17284314]
37. Scita G, Tenca P, Areces LB, Tocchetti A, Frittoli E, Giardina G, Ponzanelli I, Sini P, Innocenti M, Di Fiore PP. An effector region in Eps8 is responsible for the activation of the Rac-specific GEF activity of Sos-1 and for the proper localization of the Rac-based actin–polymerizing machine. J Cell Biol. 2001; 154:1031–1044. [PubMed: 11524436]
38. Disanza A, Mantoani S, Hertzog M, Gerboth S, Frittoli E, Steffen A, Berhoerster K, Kreienkamp HJ, Milanesi F, Di Fiore PP, Ciliberto A, Stradal TE, Scita G. Regulation of cell shape by Cdc42 is mediated by the synergic actin-bundling activity of the Eps8–IRSp53 complex. Nat Cell Biol. 2006; 8:1337–1347. [PubMed: 17115031]
39. Chiang SH, Hwang J, Legendre M, Zhang M, Kimura A, Saltiel AR. TCGAP, a multidomain Rho GTPase-activating protein involved in insulin-stimulated glucose transport. EMBO J. 2003; 22:2679–2691. [PubMed: 12773384]
40. Rosário M, Franke R, Bednarski C, Birchmeier W. The neurite outgrowth multi-adaptor RhoGAP, NOMA-GAP, regulates neurite extension through SHP2 and Cdc42. J Cell Biol. 2007; 178:503–516. [PubMed: 17664338]
41. Liu H, Nakazawa T, Tezuka T, Yamamoto T. Physical and functional interaction of Fyn tyrosine kinase with a brain-enriched Rho GTPase-activating protein TCGAP. J Biol Chem. 2006; 281:23611–23619. [PubMed: 16777849]
42. Yano H, Cong F, Birge RB, Goff SP, Chao MV. Association of the Abl tyrosine kinase with the Trk nerve growth factor receptor. J Neurosci Res. 2000; 59:356–364. [PubMed: 10679771]
43. Escalante M, Courtney J, Chin WG, Teng KK, Kim JI, Fajardo JE, Mayer BJ, Hempstead BL, Birge RB. Phosphorylation of c-Crk II on the negative regulatory Tyr^{222} mediates nerve growth factor-induced cell spreading and morphogenesis. J Biol Chem. 2000; 275:24787–24797. [PubMed: 10825157]

44. Wilkinson S, Paterson HF, Marshall CJ. Cdc42-MRCK and Rho-ROCK signalling cooperate in myosin phosphorylation and cell invasion. Nat Cell Biol. 2005; 7:255–261. [PubMed: 15723050]
45. Moriyama K, Yahara I. Human CAP1 is a key factor in the recycling of cofilin and actin for rapid actin turnover. J Cell Sci. 2002; 115:1591–1601. [PubMed: 11950878]
46. Papin J, Subramaniam S. Bioinformatics and cellular signaling. Curr Opin Biotechnol. 2004; 15:78–81. [PubMed: 15102471]
47. Nozumi M, Togano T, Takahashi-Niki K, Lu J, Honda A, Taoka M, Shinkawa T, Koga H, Takeuchi K, Isobe T, Igarashi M. Identification of functional marker proteins in the mammalian growth cone. Proc Natl Acad Sci USA. 2009; 106:17211–17216. [PubMed: 19805073]
48. Lu J, Nozumi M, Takeuchi K, Abe H, Igarashi M. Expression and function of neuronal growth-associated proteins (nGAPs) in PC12 cells. Neurosci Res. 2011; 70:85–90. [PubMed: 21238513]
49. Wills Z, Emerson M, Rusch J, Bikoff J, Baum B, Perrimon N, Van Vactor D. A Drosophila homolog of cyclase-associated proteins collaborates with the Abl tyrosine kinase to control midline axon pathfinding. Neuron. 2002; 36:611–622. [PubMed: 12441051]
50. Nakazawa T, Watabe AM, Tezuka T, Yoshida Y, Yokoyama K, Umemori H, Inoue A, Okabe S, Manabe T, Yamamoto T. p250GAP, a novel brain-enriched GTPase-activating protein for Rho family GTPases, is involved in the N-methyl-D-aspartate receptor signaling. Mol Biol Cell. 2003; 14:2921–2934. [PubMed: 12857875]
51. Impey S, Davare M, Lasiek A, Fortin D, Ando H, Varlamova O, Obrietan K, Soderling TR, Goodman RH, Wayman GA. An activity-induced microRNA controls dendritic spine formation by regulating Rac1-PAK signaling. Mol Cell Neurosci. 2010; 43:146–156. [PubMed: 19850129]
52. Wayman GA, Davare M, Ando H, Fortin D, Varlamova O, Cheng HY, Marks D, Obrietan K, Soderling TR, Goodman RH, Impey S. An activity-regulated micro-RNA controls dendritic plasticity by down-regulating p250GAP. Proc Natl Acad Sci USA. 2008; 105:9093–9098. [PubMed: 18577589]
53. Dhavan R, Tsai LH. A decade of CDK5. Nat Rev Mol Cell Biol. 2001; 2:749–759. [PubMed: 11584302]
54. Huang Q, Raya A, DeJesus P, Chao SH, Quon KC, Caldwell JS, Chanda SK, Izpisua-Belmonte JC, Schultz PG. Identification of p53 regulators by genome-wide functional analysis. Proc Natl Acad Sci USA. 2004; 101:3456–3461. [PubMed: 14990790]
55. Fritschy JM, Harvey RJ, Schwarz G. Gephyrin: Where do we stand, where do we go? Trends Neurosci. 2008; 31:257–264. [PubMed: 18403029]
56. Kirsch J, Betz H. The postsynaptic localization of the glycine receptor-associated protein gephyrin is regulated by the cytoskeleton. J Neurosci. 1995; 15:4148–4156. [PubMed: 7790902]
57. Bausen M, Fuhrmann JC, Betz H, O'Sullivan GA. The state of the actin cyto-skeleton determines its association with gephyrin: Role of ena/VASP family members. Mol Cell Neurosci. 2006; 31:376–386. [PubMed: 16376568]
58. Carlson BR, Lloyd KE, Kruszewski A, Kim IH, Rodriguiz RM, Heindel C, Faytell M, Dudek SM, Wetsel WC, Soderling SH. WRP/srGAP3 facilitates the initiation of spine development by an inverse F-BAR domain, and its loss impairs long-term memory. J Neurosci. 2011; 31:2447–2460. [PubMed: 21325512]
59. Marco EJ, Abidi FE, Bristow J, Dean WB, Cotter P, Jeremy RJ, Schwartz CE, Sherr EH. ARHGEF9 disruption in a female patient is associated with X linked mental retardation and sensory hyperarousal. J Med Genet. 2008; 45:100–105. [PubMed: 17893116]
60. Kalscheuer VM, Musante L, Fang C, Hoffmann K, Fuchs C, Carta E, Deas E, Venkateswarlu K, Menzel C, Ullmann R, Tommerup N, Dalprà L, Tzschach A, Selicorni A, Lüscher B, Ropers HH, Harvey K, Harvey RJ. A balanced chromosomal translocation disrupting ARHGEF9 is associated with epilepsy, anxiety, aggression, and mental retardation. Hum Mutat. 2009; 30:61–68. [PubMed: 18615734]
61. Kins S, Betz H, Kirsch J. Collybistin, a newly identified brain-specific GEF, induces submembrane clustering of gephyrin. Nat Neurosci. 2000; 3:22–29. [PubMed: 10607391]
62. Poulopoulos A, Aramuni G, Meyer G, Soykan T, Hoon M, Papadopoulos T, Zhang M, Paarmann I, Fuchs C, Harvey K, Jedlicka P, Schwarzacher SW, Betz H, Harvey RJ, Brose N, Zhang W,

Varoqueaux F. Neuroligin 2 drives postsynaptic assembly at perisomatic inhibitory synapses through gephyrin and collybistin. Neuron. 2009; 63:628–642. [PubMed: 19755106]

63. Papadopoulos T, Korte M, Eulenburg V, Kubota H, Retiounskaia M, Harvey RJ, Harvey K, O'Sullivan GA, Laube B, Hulsmann S, Geiger JR, Betz H. Impaired GABAergic transmission and altered hippocampal synaptic plasticity in collybistin-deficient mice. EMBO J. 2007; 26:3888–3899. [PubMed: 17690689]
64. Lee HS, Dimla RD, Schultz PG. Protein-DNA photo-crosslinking with a genetically encoded benzophenone-containing amino acid. Bioorg Med Chem Lett. 2009; 19:5222–5224. [PubMed: 19643606]
65. Gingras AC, Aebersold R, Raught B. Advances in protein complex analysis using mass spectrometry. J Physiol. 2005; 563:11–21. [PubMed: 15611014]
66. Armstrong L, Lako M, van Herpe I, Evans J, Saretzki G, Hole N. A role for nucleo-protein Zap3 in the reduction of telomerase activity during embryonic stem cell differentiation. Mech Dev. 2004; 121:1509–1522. [PubMed: 15511642]
67. Harvey K, Duguid IC, Alldred MJ, Beatty SE, Ward H, Keep NH, Lingenfelter SE, Pearce BR, Lundgren J, Owen MJ, Smart TG, Luscher B, Rees MI, Harvey RJ. The GDP-GTP exchange factor collybistin: An essential determinant of neuronal gephyrinclustering. J Neurosci. 2004; 24:5816–5826. [PubMed: 15215304]
68. Reddy-Alla S, Schmitt B, Birkenfeld J, Eulenburg V, Dutertre S, Böhringer C, Götz M, Betz H, Papadopoulos T. PH-domain-driven targeting of collybistin but not Cdc42 activation is required for synaptic gephyrin clustering. Eur J Neurosci. 2010; 31:1173–1184. [PubMed: 20345913]
69. Endris V, Wogatzky B, Leimer U, Bartsch D, Zatyka M, Latif F, Maher ER, Tariverdian G, Kirsch S, Karch D, Rappold GA. The novel Rho-GTPase activating gene MEGAP/srGAP3 has a putative role in severe mental retardation. Proc Natl Acad Sci USA. 2002; 99:11754–11759. [PubMed: 12195014]
70. Addington AM, Rapoport JL. The genetics of childhood-onset schizophrenia: When madness strikes the prepubescent. Curr Psychiatry Rep. 2009; 11:156–161. [PubMed: 19302770]
71. Lewis DA, González-Burgos G. Neuroplasticity of neocortical circuits in schizophrenia. Neuropsychopharmacology. 2008; 33:141–165. [PubMed: 17805309]
72. Enomoto T, Tse MT, Floresco SB. Reducing prefrontal g-aminobutyric acid activity induces cognitive, behavioral, and dopaminergic abnormalities that resemble schizophrenia. Biol Psychiatry. 2011; 69:432–441. [PubMed: 21146155]
73. Westphal RS, Soderling SH, Alto NM, Langeberg LK, Scott JD. Scar/WAVE-1, a Wiskott-Aldrich syndrome protein, assembles an actin-associated multi-kinase scaffold. EMBO J. 2000; 19:4589–4600. [PubMed: 10970852]
74. Durocher Y, Perret S, Kamen A. High-level and high-throughput recombinant protein production by transient transfection of suspension-growing human 293-EBNA1 cells. Nucleic Acids Res. 2002; 30:E9. [PubMed: 11788735]
75. Keller A, Nesvizhskii AI, Kolker E, Aebersold R. Empirical statistical model to estimate the accuracy of peptide identifications made by MS/MS and database search. Anal Chem. 2002; 74:5383–5392. [PubMed: 12403597]
76. Nesvizhskii AI, Keller A, Kolker E, Aebersold R. A statistical model for identifying proteins by tandem mass spectrometry. Anal Chem. 2003; 75:4646–4658. [PubMed: 14632076]
77. de Hoon MJ, Imoto S, Nolan J, Miyano S. Open source clustering software. Bioinformatics. 2004; 20:1453–1454. [PubMed: 14871861]
78. Saldanha AJ. Java Treeview—Extensible visualization of microarray data. Bioinformatics. 2004; 20:3246–3248. [PubMed: 15180930]
79. Szklarczyk D, Franceschini A, Kuhn M, Simonovic M, Roth A, Minguez P, Doerks T, Stark M, Muller J, Bork P, Jensen LJ, von Mering C. The STRING database in 2011: Functional interaction networks of proteins, globally integrated and scored. Nucleic Acids Res. 2011; 39:D561–D568. [PubMed: 21045058]
80. Schneider Gasser EM, Straub CJ, Panzanelli P, Weinmann O, Sassoè-Pognetto M, Fritschy JM. Immunofluorescence in brain sections: Simultaneous detection of pre-synaptic and postsynaptic proteins in identified neurons. Nat Protoc. 2006; 1:1887–1897. [PubMed: 17487173]

81. Ippolito DM, Eroglu C. Quantifying synapses: An immunocytochemistry-based assay to quantify synapse number. J Vis Exp. 2010 10.3791/2270.

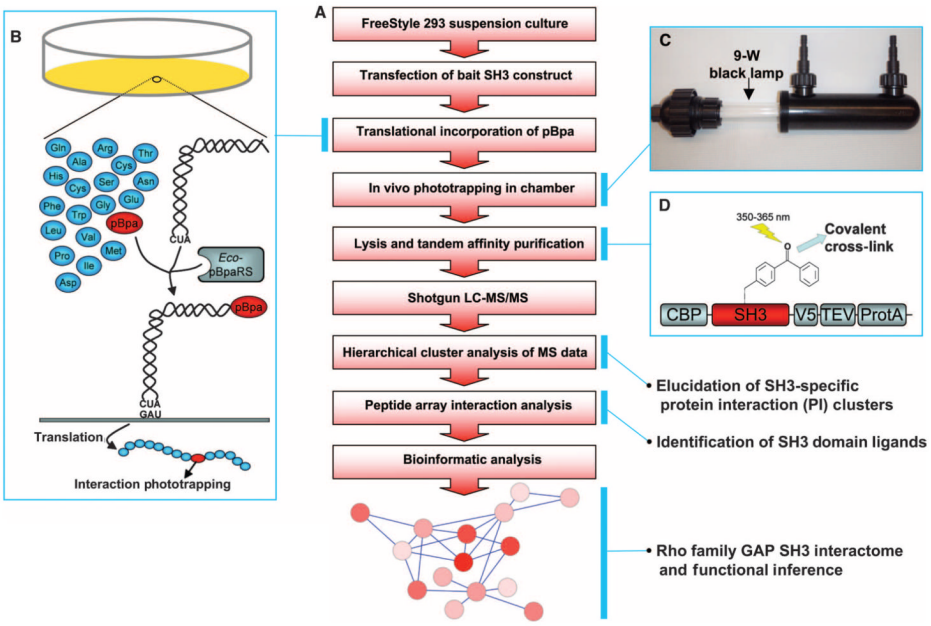

Fig. 1.

Experimental design to identify Rho family GAP protein complexes. (**A**) Workflow of overall approach to construct Rho family GAP interactomes. (**B**) Schematics for in vivo phototrapping strategy. A photo-activatable cross-linker, pBpa, is translationally incorporated into a cellular protein of interest at the site designated by an amber codon when coexpressed with a pBpa-specific tRNA synthetase and amber suppression tRNA. pBpa covalently cross-links with a binding protein when UV light is applied. (**C**) Modified cross-linking chamber for cells in suspension with inlet, outlet, and 9-W 350- to 365-nm light source. (**D**) Schematic of the SH3 domain expression construct. TAP tag (protein A, TEV protease cleavage site, and CBP) was attached to the SH3 domain for the effective isolation of SH3 domain–ligand cross-linked protein complexes. A V5 epitope was added to follow the TAP purification process.

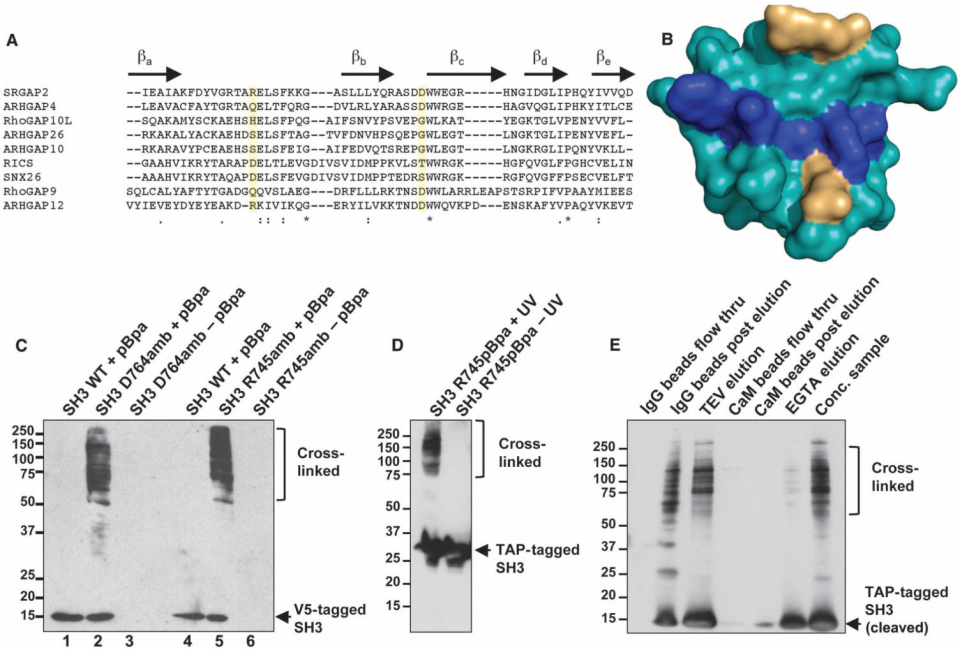

Fig. 2.

In vivo phototrapping and purification of ligands for Rho family GAP SH3 domains. (**A**) Sequence alignment of the Rho family GAP SH3 domains used in this study. Two amino acid positions (in yellow) were used to place pBpa within the SH3 domains listed. β Sheets a to e of the SH3 domain structure are indicated above. (**B**) Positions of pBpa within the structure of a Rho family GAP SH3 domain. The SH3 domain structure of SRGAP1 was used to determine the candidate residues (in yellow) to be replaced with pBpa that correspond to the residues in yellow in (**A**). Ligand-binding pocket is shown in blue. (**C**) In situ photo–cross-linking of an SH3 domain. Cells expressing V5-tagged wild-type (WT) SRGAP2 SH3 domain (lanes 1 and 4) or amber mutations (D764amb: lanes 2 and 3; R745amb: lanes 5 and 6) were grown with (lanes 2 and 5) or without (lanes 3 and 6) pBpa and subjected to UV light. Western blot analysis of the immunoprecipitates by anti-V5 antibody reveals cross-linked high–molecular weight SH3-linked protein complexes. Representative blot from $n = 2$ is shown. (**D**) Photoactivation-dependent cross-linking of an SH3 domain. Cellsexpressing TAP-tagged SRGAP2 R745amb mutation SH3 domain were in-cubated with pBpa. After 3 days, cells were exposed to UV light in a photo–cross-linking chamber. Western blot analysis reveals photo-activatedcross-linking of the SH3 domain. Representative blot from $n = 2$ is shown. (**E**) TAP of cross-linked SH3 domain protein complexes. The cell lysate obtained in (**D**) was subjected to TAP. The final eluate was concentrated bycentrifugal filtration (Conc. sample) and subjected to mass spectrometricanalysis. Representative blot from $n = 3$ is shown.

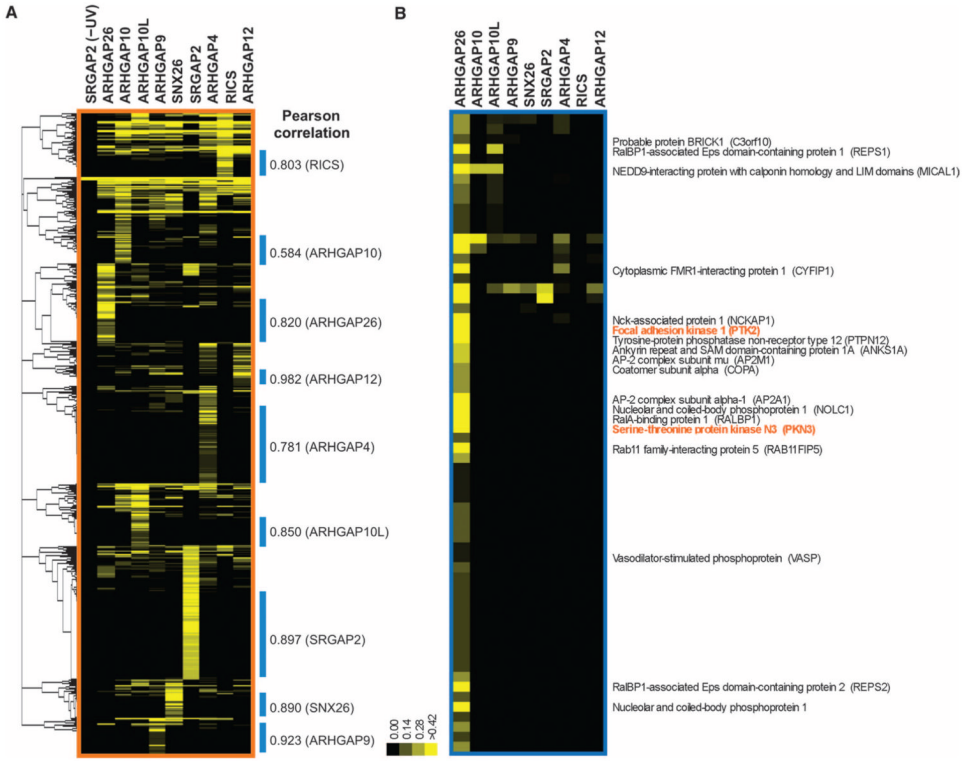

Fig. 3.

Elucidation of protein clusters enriched with Rho family GAP SH3 domains after in vivo phototrapping. (**A**) Hierarchical clustering of MS-identified SH3 domain–associated proteins. Hierarchical clustering analysis was performed with unbiased Pearson correlation of the mean normalized spectral counts for the Rho family GAP SH3 domains listed in Fig. 2. Protein clusters designated with blue bars contain proteins that predominantly associated with individual SH3 domains. The degree of correlation in each cluster is shown. (**B**) Protein cluster with a predominant specificity for the ARHGAP26 SH3 domain. Proteins that have relatively high spectral counts or have been implicated in cytoskeletal regulation are exhibited. This protein cluster contains two proteins (PTK2 and PKN3 in orange) known to interact with ARHGAP26 in an SH3 domain–dependent manner.

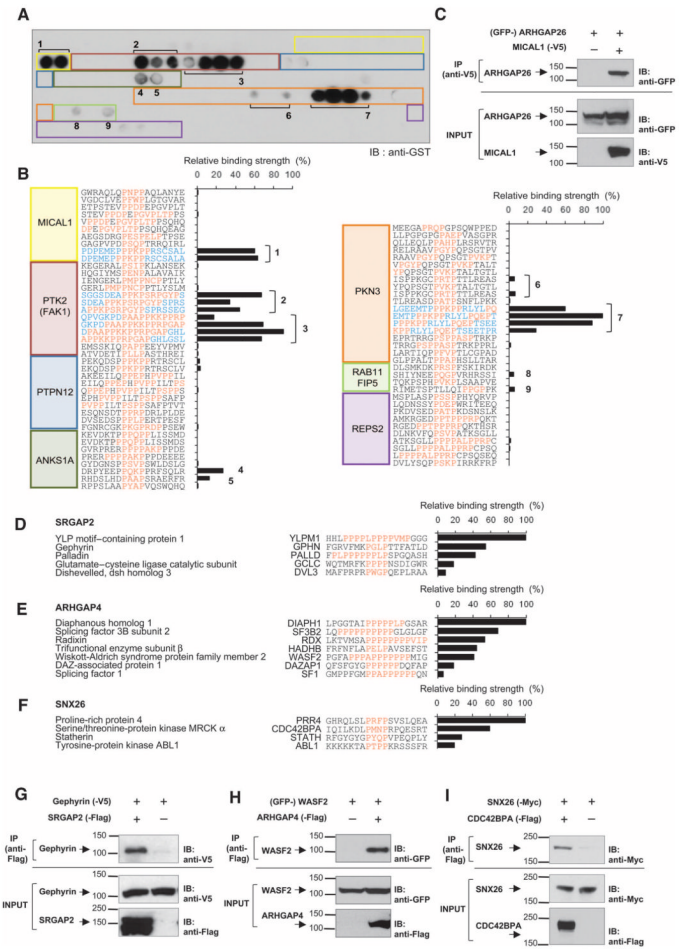

Fig. 4.

Identification of SH3 domain ligands. (**A**) Array-based binding assay to identify SH3 domain–binding peptides. Peptides (18-mer) containing PXXP motifs from proteins in the ARHGAP26 PI cluster were synthesized, incubated with purified GST-tagged ARHGAP26 SH3 domain, and immunoblotted with anti-GST antibody. Colored rectangles and numbers indicate the positions of peptides that correspond to the peptide sequences listed in (B). Representative blot from $n = 2$ is shown. (B) SH3 ligand identification and determination of relative binding strength. Peptide immunoblots generated in (**A**) were densitometrically quantified. The apparent binding strength was normalized to the strongest interaction for ARHGAP26. PXXP motifs are indicated in orange. Numbers indicate unique motifs bound to the ARHGAP26 SH3 domain with more than 5% normalized binding strength. Note that peptides overlap each other (indicated in blue) and contain the identical core motif sequences. See fig. S2, A to I, for the in vitro binding assays for all Rho family GAP SH3 domains analyzed. (**C**) Coimmuno-precipitation (IP) of full-length ARHGAP26 by MICAL1. The cell lysates of HEK293 cells expressing GFP-tagged ARHGAP26 with or without V5-tagged MICAL1 were immunoprecipitated and blotted as indicated. Representative blot from $n = 2$ is shown. (D to F) SH3 domain ligands and their binding strengths for SRGAP2, ARHGAP4, and SNX26. PI clusters specific to SRGAP2, ARHGAP4, or SNX26 were subjected to peptide array–based in vitro binding assays as for ARHGAP26. Pep-tides that showed positive binding (more than 5% normalized binding strength) to each SH3 domain are shown. (G to I) Coimmunoprecipitation experiments using

full-length Rho family GAPs. (**G**) HEK293 cells coexpressing gephyrin-V5 with vector or SRGAP2-Flag, (**H**) GFP-WASF2 with vector or ARHGAP4-Flag, or (**I**) SNX26-Myc with CDC42BPA-Flag or vector were subjected to immunoprecipitation and Western blot analysis by indicated antibodies. $n = 2$ to 4 for each coimmunoprecipitation. See fig. S2, J and K, for additional coimmunoprecipitation experiments.

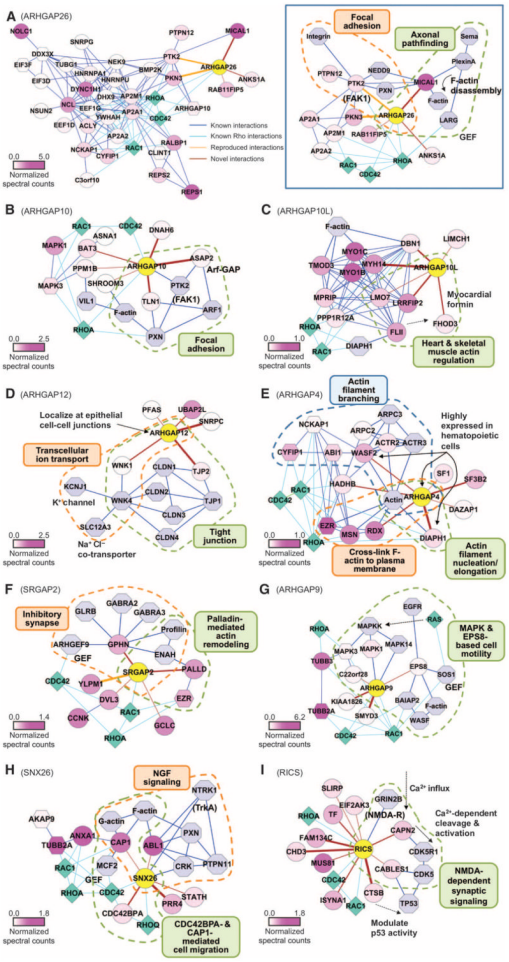

Fig. 5.

Rho family GAP interactome graphs with inferred cellular functions. Protein-protein interaction networks constructed from the interactions identified in this study and previously identified (physical) interactions. Circle nodes represent proteins in the PI clusters specific to individual SH3 domains. Hexagon nodes represent proteins that were associated with two SH3 domains but were excluded from PI clusters in the hierarchical clustering. Both nodes are colored in the purple spectrum (bottom left of each graph) reflecting the mean normalized spectral counts. Light blue octagon nodes indicate proteins identified in previous studies. Diamond nodes in cyan represent GTPases. Brown edges represent interactions identified here, and orange edges indicate known interactions reproduced in this study. Edge thickness reflects the relative binding affinity determined by in vitro binding assays. Blue and cyan edges of constant thickness indicate previously known interactions. (A, left) ARHGAP26 interactome graph. Proteins from the ARHGAP26-specific PI cluster (circle nodes) and ARHGAP26-enriched proteins (hexagon nodes) make a densely connected protein network. (See fig. S3, A to I, for other Rho family GAP interactomes.) (A to I) Graphs of Rho family GAP interactomes based on direct interactions identified in this study combined with previously known interactions to infer cellular functions. Subnetworks with specific cell functions are grouped by dashed line and indicated (see text for details).

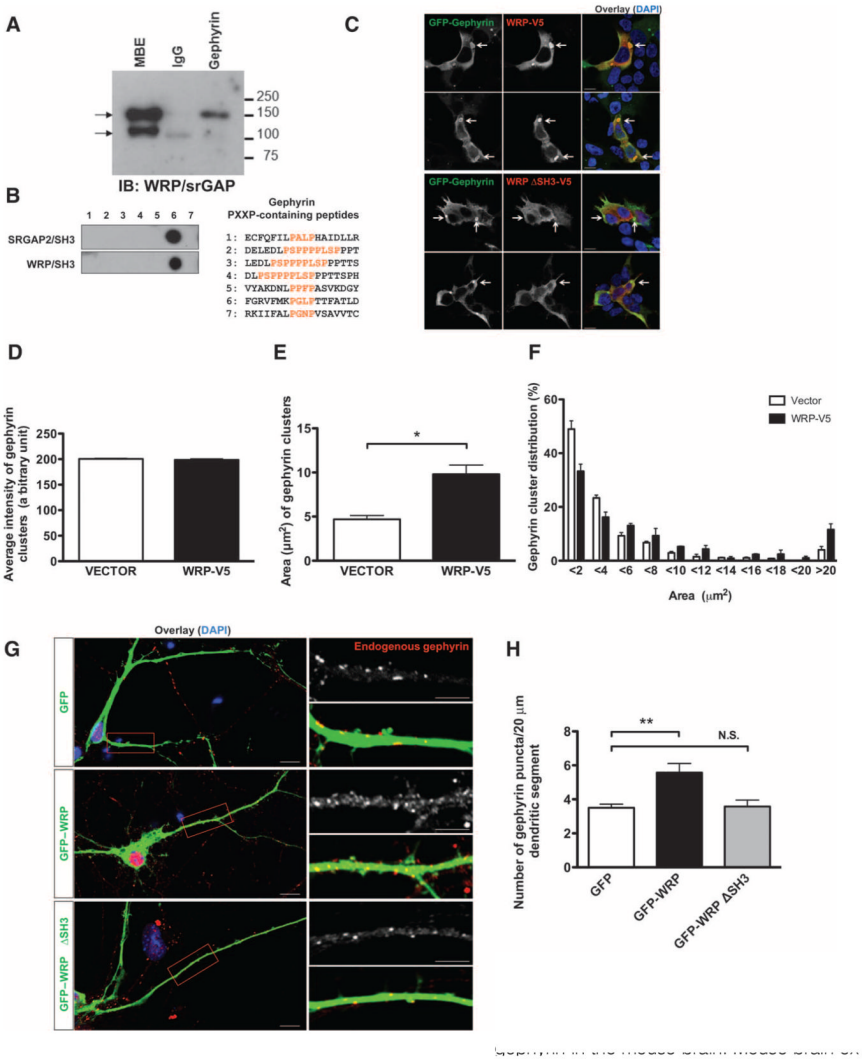

Fig. 6.

WRP enhances gephyrin clustering in HEK cells and hippocampal neurons. (**A**) Coimmunoprecipitation of SRGAP2 and WRP by gephyrin in the mouse brain. Mouse brain extract (MBE) was subjected to immunoprecipitation with anti-gephyrin antibody. Coprecipitation of SRGAP2 or WRP (indicated by arrows) was observed by Western blot using anti-SRGAP2/WRP antibody. Representative blot from $n = 4$ is shown. (**B**) SRGAP2 and WRP bind the same site in gephyrin. Gephyrin peptides (18-mer) containing PXXP motifs were synthesized, incubated with purified GST-tagged SH3 domains of SRGAP2 or WRP, and immunoblotted with anti-GST antibody. Representative blot from $n = 2$ is shown. (**C**) Colocalization of WRP with clustered gephyrin in HEK293 cells. GFP-tagged gephyrin was coexpressed in HEK293 cells with V5-tagged WRP or WRP lacking its SH3 domain. Immunofluorescence was visualized with anti-GFP (green) and anti-V5 antibodies (red), or 4′,6-diamidino-2-phenylindole (DAPI) (blue). Arrows indicate gephyrin clusters. Scale bars, 10 mm. (D to F) Increased size of gephyrin clusters upon WRP coexpression. Area of gephyrin clusters was measured in cells cotransfected with GFP-gephyrin and vector or WRP-V5. Average intensity (**D**), area (**E**), and area distribution (**F**) of gephyrin clusters from three independent experiments are shown. Data are presented as means ± SEM. $*P <$ 0.0005 (two-tailed t test). (**G**) SH3-dependent increase in endogenous gephyrin clustering by

WRP. Hippocampal neurons transfected at DIV9 with GFP, GFP-tagged WRP, or WRP lacking the SH3 domain were fixed at DIV12 and stained with anti-gephyrin antibody. Scale bars, 10 mm (left panels) or 5 mm (right panels). (**H**) Quantification of the gephyrin clusters in (**G**). GFP, $n = 42$ neurons from seven mice; GFP-WRP, $n = 27$ neurons from four mice; GFP-WRP DSH3, $n = 14$ neurons from three mice. Data are presented as means ± SEM. $^{**}P < 0.0005$ (two-tailed t test). N.S., not significant.

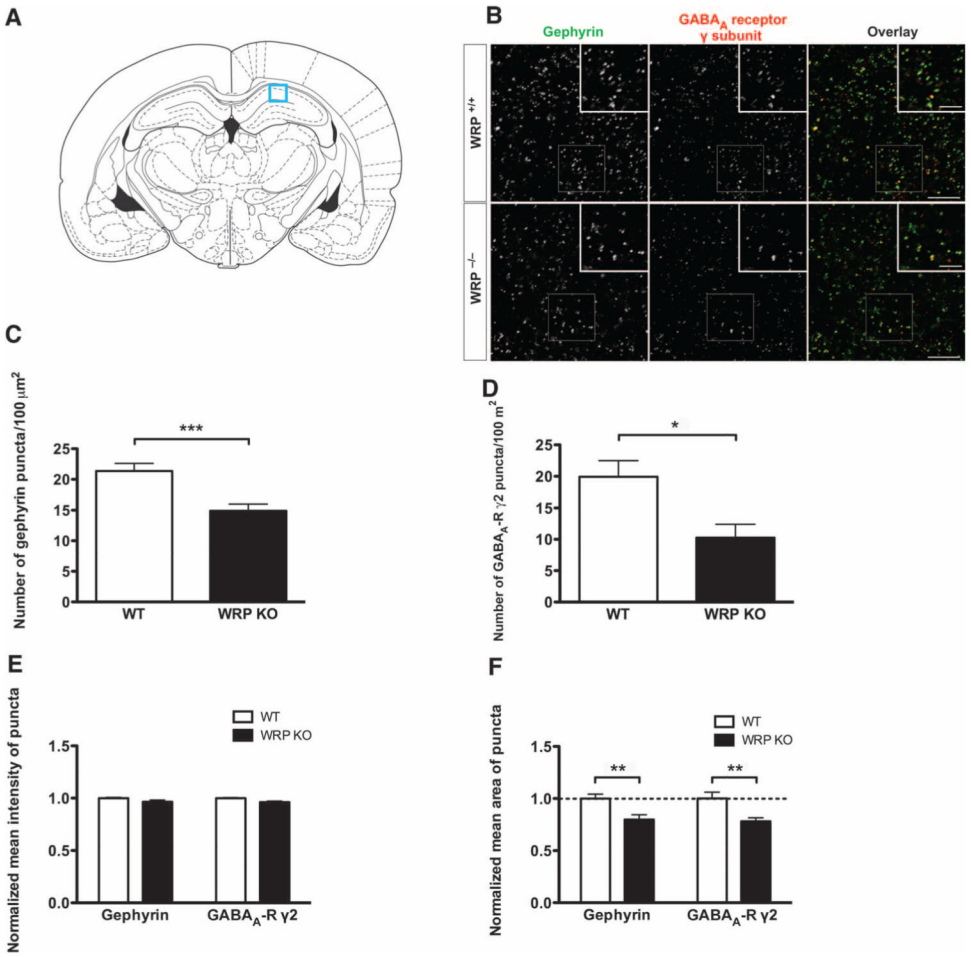

Fig. 7.

WRP promotes postsynaptic clustering of gephyrin and $GABA_A$ receptors in vivo. (**A**) Coronal section of mouse brain. Immunohistological analysis was performed on the CA1 region of the hippocampal formation (boxed region) where inhibitory synapses are made on the dendrites of pyramidal neurons. (**B**) Reduction of gephyrin cluster density and associated $GABA_A$ receptors in WRP knockout (KO) mice. Stratum radiatum of CA1 region in the hippocampal formation from $WRP^{+/+}$ or $WRP^{-/-}$ mice was stained with anti-gephyrin and anti-$GABA_A$ receptor γ subunit antibodies. (C and D) Quantification of the density of gephyrin and $GABA_A$ receptor puncta. $n = 3$ mice. From each mouse, four brain slices were processed for immunostaining and two images per slice were obtained. Data are presented as means ± SEM. ***$P < 0.0005$; *$P < 0.01$ (two-tailed t test). (**E**) Comparison of the average fluorescence intensity of gephyrin and $GABA_A$ receptor puncta. (**F**) Decreased sizes of gephyrin and $GABA_A$ receptor puncta in WRP knockout mice. Data are presented as means ± SEM. **$P < 0.005$ (two-tailed t test).

Table 1

Direct interacting proteins for each SH3 domain. Peptide sequences that bound to each SH3 domain (based on the peptide array interaction screens). Protein names and corresponding gene nomenclature as well as relative binding strengths are listed. PXXP motif for each peptide is shown in orange.

Protein name	Gene name	Accession	SH3 binding sequence	Relative binding strength(%)	Cytoskeletal function
ARHGAP26					
Serine-threonine protein kinase N3	*PKN3*	Q6P5Z2	EMTPPPKPPRLYLPQEPT	100	
Focal adhesion kinase 1	*PTK2*	Q05397	DPAAPPKKPPRPGAPGHL	91	Focal adhesion turnover
NEDD9-interacting protein with calponin homology and LIM domains	*MICAL1*	Q8TDZ2	DPEMEPPPKPPRSCSALA	64	Actin depolymerization
Ankyrin repeat and SAM domain–containing protein 1A	*ANKS1A*	Q92625	DRPYEEPPQKPPRFSQLR	27	
Rab11 family interacting protein 5	*RAB11FIP5*	Q9BXF6	RIMETSPTLLQIPPGPPK	6	
ARHGAP10					
Paxillin-associated protein with ARF GAP activity 3	*ASAP2*	O43150	GISQIRPPPLPPQPPSRL	100	Arf-GAP. Recruits paxillin to focal contacts
Dynein heavy chain 6	*DNAH6*	Q9C0G6	EKERPPKPEAPWLPTATW	95	Dynein heavy chain
Talin-1	*TLN1*	Q9Y490	RIIRERIPEAPAGPPSDF	80	Focal adhesion component
Large proline-rich protein BAT3	*BAT3*	P46379	QTLGQQVPGFPTAPTRVV	58	
Protein Shroom 3	*SHROOM3*	Q8TF72	ASDSGRGPQRPDARLLRS	37	F-actin binding. Apical constriction
Protein phosphatase 1B	*PPM1B*	O75688	FSTQDHKPCNPREKERIQ	19	
ARHGAP10L					
Myosin-14	*MYH14*	Q7Z406	AQPFLFTPRGPSAGGGPG	100	Myosin heavy chain
Drebrin	*DBN1*	Q16643	AAIIAQRPDNPREFFKQQ	68	F-actin binding
Leucine-rich repeat flightless-interacting protein 2	*LRRFIP2*	Q9Y608	YNGGLYNPYGPRTPSECS	65	Interacts with the formin-regulatory protein Flightless
FH1/FH2 domain–containing protein 3	*FHOD3*	Q2V2M9	HREAPGPPPPPPPTFLGL	53	Formin. Actin nucleation and elongation
LIM domain only protein 7	*LMO7*	Q8WWI1	LYVRKLSPVMPNPGNAFD	12	Contains actin binding calponin homology domain
LIM homology domain– and calponin homology domain–containing protein 1	*LIMCH1*	Q9UPQ0	GPFSPCSPTPPGQSPNRS	11	Contains actin binding calponin homology domain
ARHGAP12					
U1 small nuclear ribonucleoprotein C	*SNRPC*	P09234	GAMIPPPPSLPGPPRPGM	100	
Tight junction protein ZO-2	*TJP2*	Q9UDY2	FGRSILKPSTPIPPQEGE	93	Tight junction protein
Serine-threonine protein kinase WNK1	*WNK1*	Q9H4A3	NATALELPGLPLSLPQPS	52	Controls junctional ion transport by inhibiting WNK4

Protein name	Gene name	Accession	SH3 binding sequence	Relative binding strength(%)	Cytoskeletal function
Ubiquitin-associated protein 2–like	*UBAP2L*	Q14157	YSIPFPTPTTPLTGRDGS	45	
Phosphoribosylformylglycinamidine synthase	*PFAS*	O15067	FPKASVPREPGGPSPRVA	24	
ARHGAP4					
Diaphanous homolog 1	*DIAPH1*	O60610	LPGGTAIPPPPPLPGSAR	100	Formin. Actin nucleation and elongation
Splicing factor 3B subunit 2	*SF3B2*	Q13435	LQPPPPPPPPPPGLGLGF	68	
Radixin	*RDX*	P35241	LKTVMSAPPPPPPPPVIP	53	Cross-link F-actin to plasma membrane
Trifunctional enzyme subunit β	*HADHB*	P55084	FRFNFLAPELPAVSEFST	44	
Wiskott-Aldrich syndrome protein family member 2	*WASF2*	Q9Y6W5	PGFAPPPAPPPPPPPMIG	41	Arp2/3-mediated actin nucleation promoter
DAZ-associated protein 1	*DAZAP1*	Q96EP5	QFSFGYGPPPPPPDQFAP	18	
Splicing factor 1	*SF1*	Q15637	GMPPFGMPPAPPPPPPQN	7	
SRGAP2					
YLP motif–containing protein 1	*YLPM1*	P49750	HHLPPPPLPPPPVMPGGG	100	
Gephyrin	*GPHN*	Q9NQX3	FGRVFMKPGLPTTFATLD	55	Inhibitory postsynaptic scaffold protein. Associates with cytoskeleton
Palladin	*PALLD*	Q8WX93	FPLPPPPPPLPSPGQASH	43	Actinremodeling and bundling
Glutamate–cysteine ligase catalytic	*GCLC*	P48506	WQTMRFKPPPPNSDIGWR	18	
Dishevelled, dsh homolog 3	*DVL3*	Q92997	MAFPRPRPWGPQEPLRAA	9	
ARHGAP9					
SET and MYND domain–containing protein 3	*SMYD3*	Q9H7B4	NGLRAVTPLRPGELLFRS	100	
Coiled-coil domain–containing protein KIAA1826	*KIAA1826*	Q8NCY6	SRRENELPDFPHIDEFFT	70	
EGFR kinase substrate 8	*EPS8*	Q12929	PKEQFIPPYVPRFRNGWE	24	Complexes with BAIAP2 and regulates actin dynamics
UPF0027 protein C22orf28	*C22orf28*	Q9Y3I0	GSTRAFPPHHPLIAVDYQ	13	
SNX26					
Proline-rich protein 4	*PRR4*	Q16378	GHRQLSLPRFPSVSLQEA	100	
Serine-threonine protein kinase MRCK a	*CDC42BPA*	Q5VT25	IQILKDLPMNPRPQESRT	60	Cdc42-activated serine-threonine kinase
Statherin	*STATH*	P02808	RFGYGYGPYQPVPEQPLY	28	
Tyrosine protein kinase ABL1	*ABL1*	P00519	KKKKKTAPTPPKRSSSFR	20	Cytoskeletal remodeling
Adenylyl cyclase–associated protein 1	*CAP1*	Q01518	PPPPPPCPPPPPVSTISC	10	Actin binding. Regulates filament dynamics
RICS					
Cathepsin B	*CTSB*	P07858	CGTFLGGPKPPQRVMFTE	100	
Chromodomain helicase-DNA binding protein 3	*CHD3*	Q12873	YLNLSQEPAHPAMALHAR	88	

Protein name	Gene name	Accession	SH3 binding sequence	Relative binding strength(%)	Cytoskeletal function
Protein FAM134C	*FAM134C*	Q86VR2	ALVEVLGPYEPLLSRVQA	85	
Calpain-2 catalytic subunit	*CAPN2*	P17655	AGTLFQDPSFPAIPSALG	49	Proteolysis of substrates involved in cytoskeletal remodeling
Serotransferrin	*TF*	P02787	NLREGTCPEAPTDECKPV	49	
Inositol-3-phosphate synthase 1	*ISYNA1*	Q9NPH2	LSFLFKAPLVPPGSPVVN	45	
Crossover junction endonuclease MUS81	*MUS81*	Q96NY9	RSRPWGTPGNPESGAMTS	31	
Eukaryotic translation initiation factor 2-a kinase 3	*EIF2AK3*	Q9NZJ5	VRISEKFPSSPKALESVT	15	
CDK5 and ABL1 enzyme substrate 1	CABLES1	Q8TDN4	GCIALAAPGTPAAGLAAG	7	Facilitates CDK5 activation
SRA stem-loop–interacting RNA binding protein, mitochondrial	*SLIRP*	Q9GZT3	VQVHTRRPKLPQTSDDEK	7	
Vigilin	*HDLBP*	Q00341	PTYKDAFPPLPEKAACLE	5	